NTNU – Trondheim
Norwegian University of
Science and Technology

Modelling and Transient Analysis of a 10 MW Superconducting Wind Turbine Generator

Md. Rafed Hossain

Wind Energy
Submission date: December 2014
Supervisor: Arne Nysveen, ELKRAFT
Co-supervisor: Dr. Ir. Henk Polinder, TU Delft

Norwegian University of Science and Technology
Department of Electric Power Engineering

Modelling and Transient Analysis of a 10 MW Superconducting Wind Turbine Generator

M.R Hossain

Master of Science Thesis

TU Delft Delft University of Technology

NTNU Norwegian University of Science and Technology

EWEM

Modelling and Transient Analysis of a 10MW Superconducting Wind Turbine Generator

Author: M. Rafed Hossain

Master thesis submitted for fulfilling the requirements for the degree of

Erasmus Mundus
Wind Energy Masters

TU Delft

NTNU

Supervisors:

Dr. ir. H. Polinder

Prof. A. Nysveen

ir. D. Liu

Abstract

The number of installed wind turbines is growing every year as the need for energy increases in an exponential manner. As the wind turbines are trying to fulfil these requirements, the demand for output power from each individual turbine is increasing as well. Although this is great, implementation of new technologies such as direct drive superconducting generators are required as they have a great potential for becoming a great contender for satisfying the increasing demand of individual turbine power output.

The efficiency and the mass reduce by using this technology but other issues have to be checked regarding its transient performance. Due to the low sub-transient, transient and synchronous reactance, compared to a conventional machine, the transient properties such as short-circuit current, field current and electromagnetic torque is much higher. This may cause problems as high values may damage the windings and turbine properties and even cause the superconducting field windings to lose its superconducting property. The thesis report will try to model a superconducting generator for a 10MW wind turbine and analyse its transient properties. Also several important parameter calculations will be made taking into account the saturation due to iron in the generator. This simulation will be made for three different topologies of generator while taking into account their own individual generator geometry.

Acknowledgement

At first I would like to thank my family, friends and respected tutors for supporting me during the entire thesis process. I am grateful to my TU Delft supervisor Henk Polinder for giving me the opportunity to do this thesis topic under him and his valuable feedback during the entire thesis duration. He also further motivated me by allowing me to take his course A.C Machines which immensely helped me for my work. I would also like to thank my NTNU supervisor Prof. Arne Nysveen for keeping me in connection with NTNU's procedure and motivating me throughout the whole thesis.

I would also like to mention Dong Liu, who has been with me during my entire thesis project, helping me with his feedback on my work. He has also provided me help for obtaining valuable data via COMSOL and we have been working for close to make sure that the thesis project is a success and that I is heading in the right direction.

I would like to mention Zarah Glaap and Linda Gaffel in the constant support during my entire Master programme including the thesis period.

Table of Contents

Glossary

List of Figures

List of Tables

List of Symbols

β	[deg]	End angle of the field coil in degrees
α	[deg]	Start angle for the field coil
u_q	[V]	quadrature - axis voltage
u_f	[V]	Field voltage
u_d	[V]	direct- axis voltage
T_n	[N.m]	Nominal Torque
R_{sh}	[Ω]	Shield screen resistance
R_s	[Ω]	Stator resistance
R_f	[Ω]	Field resistance
P_n	[MW]	Nominal Power
M_{f_sh}	[H]	Mutual inductance between field and shield
M_{a_sh}	[H]	Mutual inductance between stator and shield
M_{a_f}	[H]	Mutual inductance between field and stator
L_{sh}	[H]	Shield inductance
L_q	[H]	q-axis inductance
L_f	[H]	Field inductance
L_d	[H]	d-axis inductance
J	[Kg.m^2]	Inertia of the machine
i_{sh}	[A]	Shield current.
i_q	[A]	q-axis current
i_f	[A]	Field current
i_d	[A]	d-axis current
h_{sy}	[mm]	Height of the armature yoke
h_s	[mm]	Armature slot height
h_{ry}	[mm]	Height of the field yoke
h_f	[mm]	Field coil height
f_m	[Hz]	Mechanical frequency
fm	[rad/s]	Initial Mechanical frequency
fi0	[rad]	Initial phase of the voltage
f	[rad/s]	Initial Stator frequency
f	[Hz]	Electrical frequency
b_t/τ_s		Ratio of slot width/slot pitch
B	[T]	Flux Density
λ_{sh}	[Wb]	Flux linkage of the shield

λ_q	[Wb]	q-axis flux linkage
λ_f	[Wb]	Field Flux linkage
λ_d	[Wb]	d-axis flux linkage

Chapter 1: Introduction

1.1 Background and Motivation

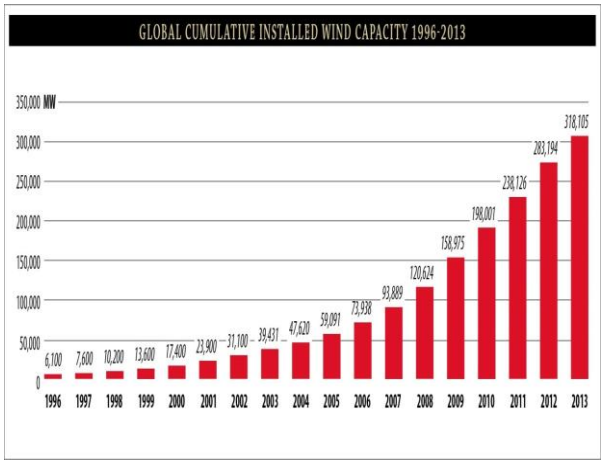

Figure 1: Global cumulative installed wind capacity 1996-2013 [1]

Renewable energy source is the next prospect for fulfilling the requirements of the vast energy needs. In today's world, wind power plays an important role in meeting this requirement. The global cumulative installed wind capacity is increasing each year and will cross the 350 GW mark in 2014 according the trend shown in Figure 1. Also according to the European Offshore Statistics, around 6.5 GW of power is produced by 2080 wind turbines in eleven European countries alone. The average offshore wind turbine size is currently at 4 MW [2]. Figure 2 shows the growth of turbine size.

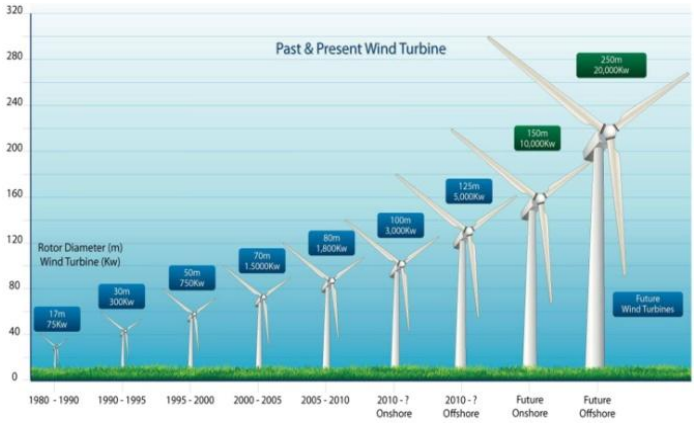

Figure 2: Past and present wind turbine size [3]

This gives a great prospect for the future trend of wind power. But an important issue, which issue which has to be considered, is the drivetrain weight that can be reached by a single turbine [4]. The combination of the weight and size of the generator and associated gearbox will require larger and more costly towers and foundations which will adversely impact payback. In addition, considering the prospects of moving beyond 10 MW of power output for a single turbine, new technologies will be required to support the growth of offshore wind market. Either to research for new materials which can withstand such stress or to make use of generator which can carry higher current density for the same amount of wind flow input.

To tackle this issue, superconducting technology may play a key role as using superconducting coils will reduce the size of the generator by up to 2-3 times while generating the same power output [5].

Although this is a great prospect, there are many factors which have to be considered for a superconducting generator (SCG).

There are several factors that provide the motivation for performing this thesis.

- Although large fault currents will occur in both conventional and SCG, the lower reactances of SCG will tend to result in larger fault currents than those which would occur in the case of a similarly-rated conventional generator.
- High values of torque may damage the mechanical parts of the turbine.
- High values of current may produce excessive heat and damage the thermal insulation [6].

1.2 Relevance and Problem definition

Whenever there is a fault in a conventional generator, the fault current is 2-3 times higher than the nominal current. This occurs during a three phase short circuit in the generator. When the same case occurs in a superconducting generator, the amount of short circuit current can be much higher in magnitude compared to that of a conventional generator. The torque is also much higher during this fault. The high value of torque might damage the mechanical parts of the wind turbine.

All of this creates a lot of problems considering that short circuit is already the most severe fault causing high torque and current in a conventional generator [7]. The high

current might also cause the superconducting material to lose its ability of superconductivity. The transient performance for a superconducting generator is thus an important issue that needs to be understood better.

This report will initially model a superconducting generator, then perform short-circuit and load change analysis for three generator topologies.

1.3 Research Objective and Thesis Structure

The main objective of this thesis is to derive a generator model for a superconducting machine and analyse its transient properties. In order to accomplish this, the following layout will be followed.

- Derive a generator model for a synchronous machine
- Obtain parameters for the three SC generator topologies chosen.
- Perform transient analysis on the models with the obtained parameters.
- Compare and analyse the results for each of the topology.

These criteria are required to be compared for each of the topology

- Short-circuit current
- Torque
- Field current

The criteria will be compared to the three generator topologies

- Iron Armature Yoke (T1)
- Iron Yokes with Air Armature Teeth (T2)
- Fully Iron Core (T3)

The parameters of these values will be used as input for the generator model and will be compared for the mentioned criteria.

The objective of this thesis will be completed in a step by step method.

Initially a system description will be provided in Chapter 2 which will describe the wind energy conversion system with brief details of the machine parts. The main focus will be given to the properties of the superconducting generator (SCG). The important components in the SCG will be described which includes the SC field windings, the cryostat and the electromagnetic shield. Some light will be shed on the fact of why a direct drive topology is used compared to the rest.

Chapter 3 will provide details on the generator model. At first, the assumptions made for modelling the generator will be mentioned. The equations which will be used to create the model will be provided. The generator model will be followed by the description of the different topologies of generator for which the transient analysis will be carried out. Before the final simulation, values such as inductance and resistance for the three topologies will be calculated, which then, will be used for the simulations.

The simulations will be described out in Chapter 4, which will compare the different generator topologies under a three phase short circuit and a load change. Values of phase current, field current, electromagnetic torque and mechanical speed will be compared for T1, T2 and T3. Results and discussion will be made for all the results obtained.

Finally, in Chapter 5, the comments will be made on the results obtained. Future recommendations, which may help further strengthen the value of this research work, will be provided briefly. The chapter will end with some final conclusions.

Chapter 2: System Description

This chapter will describe the overall wind energy conversion system with the superconducting wind turbine generator focused in details. A brief description on the drive-train will include the turbine rotor, the superconducting generator system, the generator and the grid side converter. Details of the requirements for the generator being connected to the grid will also be described with details of how the active and reactive powers are provided into the machine.

The reasoning behind the type of generator system used in this report will be mentioned. The type of superconducting materials used and the details on various components of the generator will be mentioned as well.

2.1 Wind energy conversion system

The general working principle for a wind turbine is shown in Figure 3. This shows how the source of wind is translated and converted to electrical energy in various steps. This system is directly connected to the grid through the power converter system [8] [9].

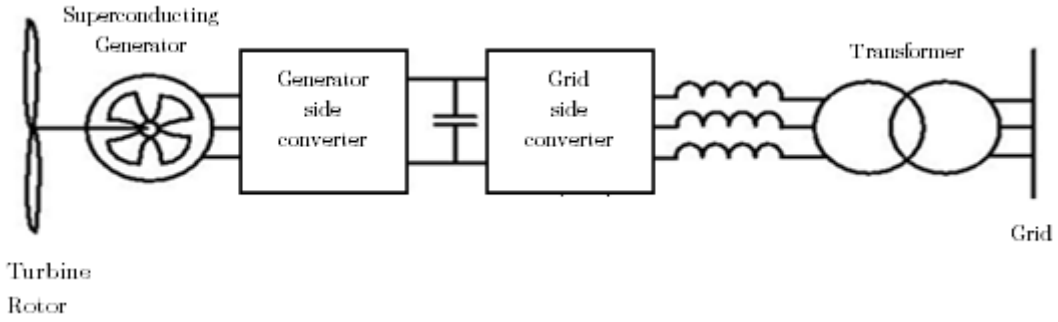

Figure 3: Wind energy conversion system

- Rotor (Hub + blades) which converts the energy in the wind to rotational shaft energy. In this report, the blades are not used directly for any part of the modelling.
- Generator as described earlier converts the mechanical energy into electrical energy. This part is going to be the main research work for this report. A direct drive superconducting generator system (DDSCG) will be used in this report.

- Generator side converter: The main function of the generator side controller is to track the maximum power from wind through controlling the rotational speed of the turbine. In this report a d-q voltage controller is made for obtaining the maximum power. This will be discussed briefly in Chapter 4.
- DC link capacitor: This provides a decoupling between the two converters meaning it separates the control between the two converters. This will not be modelled in this report for simplification during transient analysis.
- Grid side converter: It has usually both an active and a reactive power controller. It also maintains the dc-link voltage at the desired value by exporting active power to the grid and it controls the reactive power exchange with the grid. The active power is controlled by pitching the blades as described in section 2.1.2. The reactive power controller is not used in this report.
- Inductive filter and transformer: The inductive filter limits the harmonic current injection into the grid. The transformer is used for grid connection. This will not be modelled in this report.

There are important drivetrain models which will be described before further proceeding.

The wind turbine has several important components and some will be discussed briefly.

- Turbine rotor and pitch controller
- Superconducting wind turbine generator

The connection if the wind turbine with the grid will also be mentioned as there are several factors that have to be met.

2.1.1 Wind turbine rotor

The wind turbine provides the mechanical torque into the machine and acts as the prime mover. It is very important to understand this concept as this plays an important role for modelling the generator. [10]

At first, the total power (P_w), which is available from the wind source is given in eq. (2.1).

$$P_w = \frac{1}{2}\rho A u^3 \tag{2.1}$$

The total power, P_m, which is extracted by the rotor turbine from the wind source, is shown in eq. (2.2). The optimum tip speed ratio (λ_{opt}) is given in equation (2.3).

$$P_m = P_w . C_P(\lambda, \beta) \tag{2.2}$$

$$\lambda_{opt} = \frac{R w_m}{u_{rated}} \tag{2.3}$$

Where

- C_p: Turbine power coefficient ratio of power extracted by the turbine (P_m) to the total contained in the wind resource (P_{m_rated}=10 MW)
- ρ: Air density of value 1.225 kg/m^3.
- A: Turbine sweeping area (m^2) with the value πR^2. The radius of the blades is given as 95 m .
- u: wind speed. The rated speed is 11.5 m/s.
- w_m: The angular velocity of the turbine is given as 1.01 rad/s at rated condition.
- λ_{opt}: tip speed ratio of the wind turbine. It is calculated to be 8.3 at rated condition.
- β: Blade pitch angle of for the turbine [°].
  (Note: C_p is maximum when $\beta = 0$ and λ_{opt})

The rated power that is available at the rated speed is P_{w_rated}.

Where it is calculated to be (from eq. 2.1),

$$P_{w\_rated} = 26.4\ MW$$

The mechanical power that is obtained from the wind source depends on the power coefficient, C_p. This value depends on the tip speed ratio, λ, and the blade pitch angle, β, of the turbine. It is already known that the rated power that is obtained from the turbine rotor is given as:

$$P_{m\_rated} = 10\ MW$$

Since the machine is running at rated conditions with $\beta = 0$, the maximum power coefficient, C_{p_max}, value is given as:

$$C_{p\_max} = \frac{P_{m\_rated}}{P_{w\_rated}} = 0.38$$

The mechanical equation of the machine is represented by the mechanical torque T_m, electromagnetic torque T_e, and the mechanical speed w_m, where J_{TOT} is the inertia of both the generator, J_{gen} and the turbine blades J_{blades}.

$$T_m = \frac{P_m}{w_m} \tag{2.4}$$

$$J_{TOT} \frac{dw_m}{dt} = T_m + T_e \tag{2.5}$$

$$J_{TOT} = J_{blades} + J_{gen} \tag{2.6}$$

Where,

$$J_{TOT} = 6 \times 10^7 \ [kg.m^2]$$

$$J_{blades} = 5 \times 10^7 \ [kg.m^2]$$

$$J_{gen} = 5 \times 10^7 \times 0.2(approx.) = 1 \times 10^7 \ [kg.m^2]$$

It should be noted that the inertia of the generator has been accounted to be 20% of the total inertia of the turbine blades.

The electromagnetic torque must be equal to and by opposed by a mechanical torque for the wind turbine to operate at a constant rotational speed or steady state. If T_e is greater than T_m, the mechanical speed of the rotor will slow down, while if T_e is less than T_m then the rotor speed will speed up.

In this report, the generator is running at full load conditions before any of the transient period. Therefore, the P_m has a value of 10 MW.

2.1.2 Pitch controller

The pitch controller is used to control the active power in the machine. Due to the fluctuating nature of the wind the power output obtained from the wind turbine varies accordingly. This is a good option until the wind speed becomes too high [11].

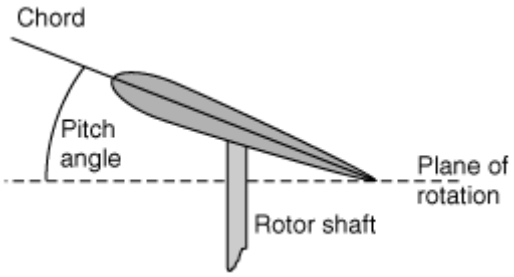

Figure 4: Blade pitching during high wind

Fatigue damage can occur to the mechanical parts of the turbine when the wind speed is too high. Thus, this might even break the blades and cause disruption to the flow of power. This issue can be solved by controlling the pitch angle of the blades. This regulates the power delivered by the rotor by pitching the blade by an angle, β. Figure 4 represents the blade pitching of a wind turbine.

As the wind speed reaches its rated value the pitch controller comes into action by increasing the angle. The rotor power coefficient, C_p, is inversely proportional to that of the pitch angle, β thus the torque, T_m, is kept constant with speed higher than the rated value until the wind speed reaches the cut out value, where the turbine stops. In simple words, this allows the turbine to produce a constant maximum power output for wind speed higher than nominal speed and stop when the wind speed reaches the rated value. The pitch controller also acts as the active power controller for the grid side converter.

Instead of modelling a full pitch controller, a simpler model is used to simulate the change in T_m. This will be described in Chapter 4.

Since the pitch controller cannot play a role during a three phase short circuit due to its slow response compared to the fault time, it is only used during the load rejection simulation.

2.1.3 Field exciter

The field exciter is the power source of the generator control system. It is the power source that supplies the dc magnetizing current to the field windings of a synchronous generator thereby ultimately inducing ac voltage and current in the generator armature [12].

In the generator model for this report, a constant field voltage, u_f, is provided into the machine.

During a three phase short circuit, the exciter cannot play any role since the fault occurs in a very short time and is not fast enough to act on it.

2.2 Superconducting Generator for wind turbines

2.2.1 Superconductivity

Superconductivity was discovered in 1911 by Heike Kamerlingh Onnes. He found that at certain temperatures some materials showed zero resistivity. That temperature is the critical temperature, T_c, of a material is the temperature at which it becomes superconducting. Superconducting magnets are first made in 1961 and soon the idea of incorporating into the electrical devices was proposed. Today, a wide range of applications are using superconductivity. Figure 5 represents the various conditions which should be met for a material to be superconductive. They are given as follows:

- The material must be cooled below a characteristic temperature, known as its superconducting transition or critical temperature (T_c) [13].
- The current passing through a given cross-section of the material must be below a characteristic level known as the critical current density (J_c).
- The magnetic field to which the material is exposed must be below a characteristic value known as the critical magnetic field (H_c)

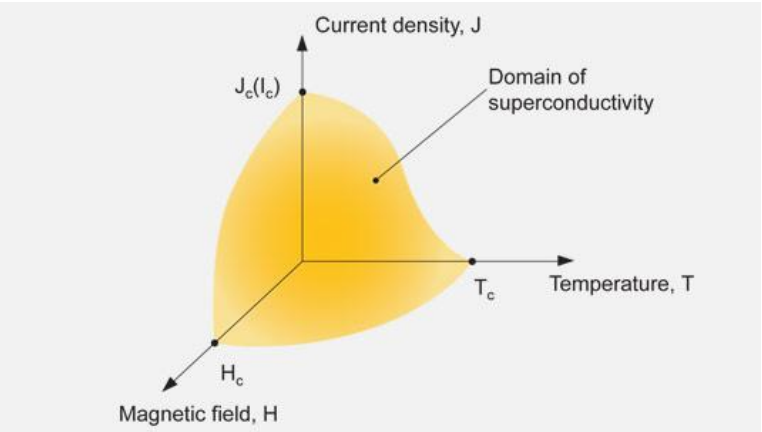

Figure 5: Conditions required for superconductivity.

The advantages and limitations of superconductors are as follows

- Advantage 1: Superconducting material can carry much higher currents with no energy loss to resistance while creating larger magnetic fields
- Advantage 2: Machines using superconducting materials will be smaller in size compared to conventional machines with the same power rating with higher efficiency [14].
- Limitation 1: Superconductors are very sensitive to high currents. At high currents, superconductors can lose its functionality which can easily revert back to normal conductors.
- Limitation 2: The superconductors developed till now can only exist in temperatures far below sub-zero. This makes is difficult to use in many applications and hard to analyse its property [15] [16].

Although the limitations are there, the prospect for superconducting generators for wind turbines are quite high in the future due to their high current carrying capability.

2.2.2 Superconducting generator

Superconducting machines have been proposed for wind turbines by both industry and academia due to their potential for high torque density and efficiency compared to conventional electrical machines. They operate with higher air-gap flux densities due to higher magnetomotive force (MMF) created by the superconducting wires that it can conduct (e.g SC wire can carry 100 A/mm^2 compared to 5-6 A/mm^2 by a copper coil).

Superconductors exhibit almost zero resistance and are therefore commonly proposed for field windings inside the generators. With a vanishing dc resistance, the resistive losses will be suppressed and the field current can be increased, such that air-gap flux densities of 2–3 T can be achieved. Therefore, superconducting machines have very high torque densities. Using the volume of a superconducting machine can be reduced by a factor of 2–3 compared with a traditional machine with an air-gap flux density just below 1 T [17].

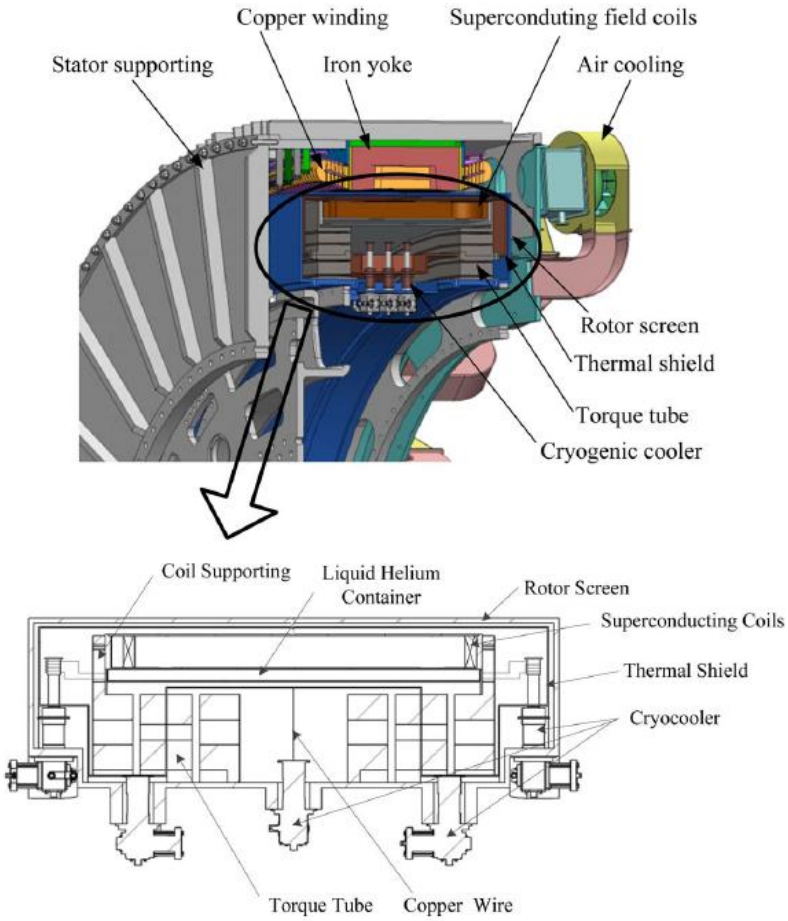

Figure 6: Configuration of a typical synchronous generator employing superconducting field winding on the rotor

If the current density, J_{Cu}, on the stator is kept constant as the machine is reduced in size, the copper losses, P_{Cu}, will be proportional to the volume of copper, V_{Cu}, and hence will reduce as the generator becomes smaller in size.

This leads to an increased efficiency for the superconducting generator compared to a conventional generator.

If these critical values are not reached, the SC machine can perform very well compared to other conventional machines [18]. Figure 6 shows the configuration of a typical synchronous generator employing superconducting field winding on the rotor.

The SCG has field windings made of the superconducting material MgB_2 in the rotor of the wind turbine generator [19].

2.2.3 Superconducting Material- MgB_2

The research in this report adopts MgB_2 tape wires to construct a field winding. Interest in MgB_2 superconductor is ever increasing, for technological applications around 10-20 K. MgB2 has higher T_C than low temperature superconductors (LTS) and less expensive than high temperature superconductors (HTS) [20]. The current carrying capacity of this material improves significantly as the temperature is reduced far below the critical temperature of 39 K. The conductors have much better mechanical properties as well for practical applications [21].

Since the material is not as expensive as its other substitutes and is relatively easy to manufacture, MgB_2 is a suitable material to be chosen for the superconducting generator in this report [22].

2.2.4 Superconducting Field Winding

The superconducting field winding is energized with DC and is designed to generate a magnetic field in the stator armature region. The stator windings experience this field as AC when the rotor rotates. In a generator this AC field produces voltage in the stator coils. The field experienced by the stator imposes following requirements on the field winding design [23]:

- Only the fundamental component of the field generated by the field winding is useful for producing power.
- Any space harmonics created by the field winding will generate harmonic voltages in the stator coils and additional eddy – current heating in coils and other metallic components. Thus these space harmonics must be minimized.
- Field winding must be designed to achieve the highest possible current density in order to minimize space used on the rotor and to minimize use of expensive superconductor.
- Cooling of superconductor winding must be adequate to minimize the temperature rise that can occur under the normal and fault conditions that must be sustained by the machine.
- Mechanical stresses within the winding and associated support structure must be acceptable during the cool - down from the room temperature to the cryogenic operating temperature and during the warm - up to the room -

temperature. The winding must also be capable of withstanding stresses under steady - state and fault conditions.

2.2.5 Cryostat and Electromagnetic (EM) Shield

The superconducting field winding in its cryogenic environment must be protected from the heat radiated and conducted from room - temperature environment. Some key features of the cryostat are as follows [24]:

- The room - temperature wall of the cryostat is mechanically tied to the shaft of the machine.
- In some cases an intermediate - temperature (between the cryogenic and room temperature) EM shield is employed to intercept any thermal loads from the stator caused by the harmonic fields.
- The space between the warm and cold walls of a cryostat is usually evacuated and filled with multi - layer insulation (MLI), as is used for minimizing the thermal radiation from the warm surfaces to cold surfaces.
- Besides torque tubes, any other mechanical connections between the cold mass and warm cryogenic wall must be optimally designed to minimize any thermal conduction into the cold environment of the field winding.

A superconducting machine needs an EM shield to protect the superconducting field winding from the asynchronous fields produced by armature currents. Besides attenuating the AC fields, an EM shield must be capable of withstanding very large torques and forces experienced by it during a transient short circuit fault. This shield is also subjected to large torque and forces during transient faults such as short - circuit on or near machine terminals.

Since the space is limited inside the generator, the cryostat is made in such a way inside the superconducting generator that it also acts as the EM shield constructed from high-conductivity aluminium or copper to provide needed attenuation of AC fields.

However, these HC metals are not sufficiently strong to bear fault torques and forces. It is also not advisable to increase the thickness of the aluminium or copper EM shields for this mechanical reason because a thicker shield lowers the damping torque during a fault.

In this report, the thickness of the cryostat, which also acts as the EM shield, is given to be 10 *mm.* Figure 6 shows how the shield is placed right between the stator and the rotor.

2.2.6 Direct Drive Superconducting Generator (DDSCG)

Direct drive superconducting generator (DDSCG) are new and strong candidates for 10 MW class wind generators. While a 10 MW permanent magnet direct drive generators (PMDD) are above 300 tons and diameters larger than 100 m for 5 MW when compared DDSCG to this case they are almost 50% lighter and are superior in terms of volume and weight for a turbine above 8 MW [25]. Thus to increase the efficiency and reliability of the system, to reduce the weight of the nacelle and price of installation, the direct-drive generator concept is adopted. DDSCG also avoids the necessity of a gearbox thus removed the possibility of a gearbox failure.

Table 1 represents the generator concepts which are used and proposed for the future for wind turbines producing 10MW and beyond.

Table 1: Direct drive transmission for 10 MW and beyond

Manufacturer	Transmission	Generator
Siemens Wind Power	Direct Drive	PMSG 6.0MW
Vestas	Medium Speed	PMSG 7.0MW
Alstom	Direct Drive	EESG 7.5MW
REPower	High Speed	DFIG 6.2MW
Areva	Low Speed	PMSG 5.0MW
10 MW and beyond- proposals/ investigation		
Manufacturer	Transmission	Generator
American Superconductor	Direct Drive	HTS 10MW
General Electric	Direct Drive	LTS 10-15MW
Advanced Magnet Lab	Direct Drive	MgB_2 10MW

It can be seen that the transmission methods are all using and proposing direct drive transmission due to it being gearless and having less mass [26] [27].

2.3 Conclusion

This chapter described the WECS on which the generator is based and modelled upon. The system is connected to the grid via the power converters. Thus the frequency and terminal voltages of the machines must be the same as the grid.

In this report the modelling of the converters has been simplified and more effort is put on the generator modelling for this machine. The two main transient characteristic that will be performed (Three phase short circuit and load rejection) occur at full load conditions. Thus it can be assumed that T_m, T_e, P_m and w_m are at rated values before the transient occurs.

Chapter 3 describes the generator model in detail.

Chapter 3: Generator Model

A generator is an electromechanical machine composed of a static part (the stator) and a rotating part (the rotor) whose relative position is changed periodically by rotating angle. This report uses a direct-drive synchronous superconducting generator as mentioned earlier (DDSSG). In general, synchronous machines can be catalogued into two types according to air gaps between stator and rotor [28] [29]:

- Synchronous machine with uniform air gaps and concentric cylindrical rotor, such as surface mount permanent machine.
- Synchronous machine with non uniform air gaps, such as salient pole of machine, interior permanent machine (IPM), etc.

In this report, the machine is considered to have uniform air gaps and concentric cylindrical rotor (non-salient pole). Therefore the model of a synchronous generator with non-salient pole will be made for analysing the superconducting machine.

3.1 Assumptions

While modelling the generator from the differential equations, several assumptions are taken into account and also considered while the calculation of the parameters. The assumptions are as follows:

- The rotor inner side is circular cylindrical.
- The effects of the slots in the stator are neglected.
- The windings in the stator are distributed sinusoidally along the circumference.
- The generator is connected with the grid thus the voltage and frequency are fixed by the grid.

The reason it is assumed to be sinusoidal is because the differential equations, which are used in the report, only takes into account the fundamental component without taking into account any harmonics [30]. This allows the user to obtain the fundamental value of the flux density and flux linkage from which the value of inductance can be calculated. This will be described in detail later in the report.

3.2 Dynamic Generator Model

The reference frame theory plays an important role to the analysis of different electric machines. All analysis presented here are based on the reference frame theory.

The model of a basic two pole salient pole synchronous superconducting machine with shield windings is shown in Figure 7. The direct axis is aligned with the N-pole of the rotor and quadrature axis is 90 degree apart from d axis.

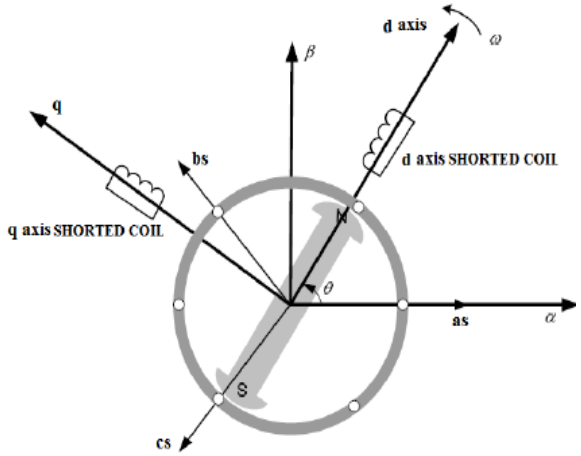

Figure 7: d & q axis position in a two pole synchronous machine

Two-pole machine is shown above; a multi-pole machine with any number of pairs of poles can be treated as a two-pole machine electrically, because armature (stator) windings are identically arranged with respect to each pair of poles.

The rotor has two axes of mechanical rectangular symmetry and they are called direct axis or d-axis and quadrature axis or 'q-axis' [31]. Namely:

- d-axis or direct-axis: the axis from the axial centre point in the pole direction.
- q-axis or quadrature-axis: the axis from the axial centre point in the direction 90^{o} ahead (leading) of the d-axis in the middle of the two poles

The field winding is a connected to a source of d.c. voltage (V_f) and with an inductance to produce flux only in the direction of the d-axis.

In this report, the concept for modelling a conventional synchronous generator is used to make the superconducting synchronous generator system.

3.2.1 Voltage and flux equations

The voltage and the flux equations are the foundation for modelling conventional synchronous generator model. They are based on a conventional generator model and are modified later to suit the requirements for an SC generator.

$$u_d = R_s i_d - \ pw_m \lambda_{\mathrm{q}} + \frac{\mathrm{d}\lambda_{\mathrm{d}}}{\mathrm{dt}} \tag{3.1}$$

$$u_q = R_s i_q + \ pw_m \lambda_{\mathrm{d}} + \frac{\mathrm{d}\lambda_{\mathrm{q}}}{\mathrm{dt}} \tag{3.2}$$

$$u_f = R_f i_f + \frac{\mathrm{d}\lambda_{\mathrm{f}}}{\mathrm{dt}} \tag{3.3}$$

$$0 = R_{\mathrm{sh}} i_{shd} + \frac{\mathrm{d}\lambda_{\mathrm{sh}}}{\mathrm{dt}} \tag{3.4}$$

$$0 = R_{\mathrm{sh}} i_{shq} + \frac{\mathrm{d}\lambda_{\mathrm{sh}}}{\mathrm{dt}} \tag{3.5}$$

Equations- 3.1 to 3.5 represent the voltage equations for the d-axis, q-axis, field windings and the electromagnetic shield. Since the machine is non-salient, d and q axis values are equal [32]. These equations form the base for designing a full synchronous generator and will be thoroughly used throughout the report [28].

$$\lambda_d = \ L_d i_d + M_{a\_f} i_f + M_{a\_shd} i_{\mathrm{shd}} \tag{3.6}$$

$$\lambda_f = \ L_f i_f + M_{a\_f} i_d + M_{f\_\mathrm{shd}} i_{\mathrm{shd}} \tag{3.7}$$

$$\lambda_{\mathrm{shd}} = \ L_{\mathrm{shd}} i_{\mathrm{shd}} + M_{f\_\mathrm{shd}} i_f + M_{a\_shd} i_{\mathrm{shd}} \tag{3.8}$$

$$\lambda_q \ = \ L_q i_q + M_{a\_shq} i_{\mathrm{shq}} \tag{3.9}$$

$$\lambda_{\mathrm{shq}} = \ L_{\mathrm{shq}} i_{\mathrm{shq}} + M_{a\_\mathrm{shq}} i_{\mathrm{shq}} \tag{3.10}$$

$$\mathrm{P} = \ u_{\mathrm{d}} i_{\mathrm{d}} + u_q i_q \tag{3.11}$$

$$\mathrm{Q} = \ u_{\mathrm{q}} i_{\mathrm{d}} - u_d i_q \tag{3.12}$$

$$\mathrm{T_e} = \ p.(\lambda_d i_{\mathrm{q}} - \lambda_q i_d) \tag{3.13}$$

Equations- 3.6 to 3.10 again represents for the d-axis, q-axis, field windings and the shield flux linkage values. These equations are based upon the assumption that the windings are sinusoidally distributed. The active and reactive powers are represented

by Equation 3.11 and 3.12. The electromagnetic torque is represented by Equation 3.13, where p represents the number of pole pairs.

3.2.2 Equivalent circuits

Figure 8 represents the equivalent circuit for a synchronous machine in the d-q axis frame. It has to be remembered that since there is no saliency in the following SC synchronous generator thus the value of the d-q axis inductances are equal.

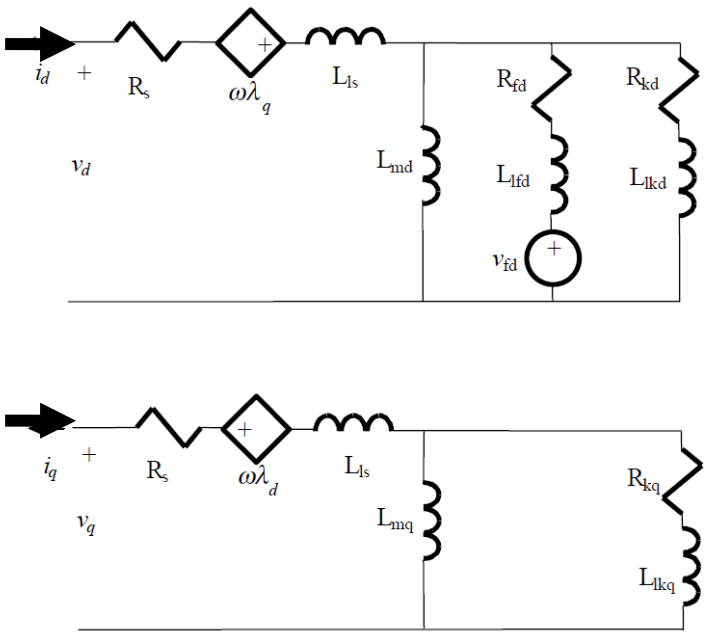

Figure 8: d-q axis equivalent circuit synchronous generator [32]

The equations for voltage and flux describe the synchronous generator's equivalent circuit in the rotor reference frame.

3.3 Generator Parameters

The generator specifications are given accordingly starting from the phase voltage to the radius of the stator bore. Inductance and resistance values are calculated using a combination of both analytical and numerical methods.

It can be seen from the equivalent circuit that there are a lot of machine parameters, which includes resistance and mainly the inductance values of the circuit.

Inductance values are obtained by using FEM which will be described later in the chapter. The reason, as mentioned earlier, is due to the saturation effect provided by the iron in the machine which makes the inductance values non-linear. The FEM method allows for obtaining a more accurate value of inductance due to saturation and thus will give more accurate simulation of the transient performance. There are three models of different generator topologies that are modelled.

Table 2: Inductance Matrix

L_d	0	M_{a_f}	M_{a_sh}	0
0	L_q	0	0	M_{a_sh}
M_{a_f}	0	L_f	M_{f_sh}	0
M_{a_sh}	0	M_{f_sh}	L_{sh}	0
0	M_{a_sh}	0	0	L_{sh}

Table 3: Resistance Matrix

R_a	0	0	0	0
0	R_a	0	0	0
0	0	Rf	0	0
0	0	0	R_{sh}	0
0	0	0	0	R_{sh}

It can be seen in Table 2 and 3 how the inductance and the resistance matrix are distributed. The matrices for both the inductance and resistance are obtained from the voltage and flux equations.

Table 4: Generator constants

Constants	Value
Nominal Power	10MW
Phase Voltage	3.3kV
Nominal torque	T_N=9.9 MNm
Number of phases	m=3
Number of slots per pole per phase	q=2
Armature current density amplitude	J_s=3 A/mm^2
Armature winding fill factor	k_{fil}=0.7
Effective air gap length	g_{eff}=40 mm
Armature bore radius	r_s=2.5 m

The generator constants on Table 4 are the same for all the three generator topologies that will be modelled.

3.3.1 Initial conditions

There are several initial values which have been calculated and assumed while modelling the generator and played a vital part during both full load and transient performance.

From the given generator parameter, the rated current is calculated to be approximately 1750A. With this value, i_d and i_q are calculated accordingly using the Park's transformations as shown in Equation 3.14

$$\begin{bmatrix} x'_d \\ x'_q \\ x'_0 \end{bmatrix} = \begin{bmatrix} \cos p\theta & \sin p\theta & 0 \\ -\sin p\theta & \cos p\theta & 0 \\ 0 & 0 & 1 \end{bmatrix} \frac{\sqrt{2}}{\sqrt{3}} \begin{bmatrix} 1 & -\frac{1}{2} & -\frac{1}{2} \\ 0 & \frac{\sqrt{3}}{2} & -\frac{\sqrt{3}}{2} \\ \frac{1}{\sqrt{2}} & \frac{1}{\sqrt{2}} & \frac{1}{\sqrt{2}} \end{bmatrix} \begin{bmatrix} x_a \\ x_b \\ x_c \end{bmatrix}$$
$$= \frac{\sqrt{2}}{\sqrt{3}} \begin{bmatrix} \cos p\theta & \cos(p\theta - \frac{2}{3}\pi) & \cos(p\theta - \frac{4}{3}\pi) \\ -\sin p\theta & -\sin(p\theta - \frac{2}{3}\pi) & -\sin(p\theta - \frac{4}{3}\pi) \\ \frac{1}{\sqrt{2}} & \frac{1}{\sqrt{2}} & \frac{1}{\sqrt{2}} \end{bmatrix} \begin{bmatrix} x_a \\ x_b \\ x_c \end{bmatrix} \quad (3.14)$$

Both i_d and i_q are calculated to be 0A and -3031A from the transformation from i_a, i_b and i_c.

At t=0, assuming steady state conditions.

Given inertia for T1, T2 and T3 [N.m]

$$J = 6.01X10^7 \text{ [N.m]}$$

This is the value which is provided by the rotor data if the reference wind turbine [referred to www.inwind.eu] and is used throughout the report.

Initial phase of voltage [rad]

$$fi0 = \frac{\pi}{2} \ [rad]$$

The value of the initial phase of the voltage makes sure that the rotor is initially aligned with the d-axis and perpendicular to the q-axis.

Initial mechanical speed [rad/s]

$$w_m = \frac{rpm}{60} * 2\pi \tag{3.15}$$

With a given rpm value of 9.65, the initial mechanical speed is the speed of the machine which is 1.01 rad/s.

Electrical frequency [rad/s]

$$w_e = w_m * p \tag{3.16}$$

Initial excitation field current

$$I_f = \frac{\sqrt{3}.U_s}{2\pi.f.M_{sf}} \tag{3.17}$$

The initial excitation current is calculated analytically and resembled with the value calculated by field winding geometry and operating field current density (J_f).

Initial excitation voltage

$$u_f = I_f R_f \tag{3.18}$$

Using the excitation current, the initial excitation voltage can be obtained by using Equation 3.18. This is used in the generator model and is kept **constant** during short circuit and load rejection.

The d-q axis voltage is represented by the eq. 3.19 and 3.20

$$u_d = R_s i_d - \ pw_m \lambda_{\mathrm{q}} \tag{3.19}$$
$$u_q = R_s i_q + \ pw_m \lambda_{\mathrm{d}} \tag{3.20}$$

The steady state voltages of d and q axis are calculated by using the inductance and the current values corresponding to d and q axis. The initial values are calculated by using Equation 3.19 and 3.20.

A model of the generator is made using fundamental dynamic models for a synchronous generator. The *MATLAB/ SIMULINK* model is shown in Appendix A.

3.4 Inductance and Resistance calculation method

For calculating the inductance and resistance, there are several steps that are carried out, especially for the inductance values.

For T1, T2 and T3 the content of iron increases for each topology and the model become more non-linear due to saturation thus requiring the need of numerical calculation for inductances.

3.4.1 Finite element method for superconducting machines

Iron is non-linear. In conventional machines, the saturation is not heavy so it can be assumed to be a linear iron in an analytical model. In superconducting machines, the iron is heavily saturated so that a linear iron cannot be assumed. There are certain limitations faced by the conventional models compared to that of a superconducting model [14] [16]. For example, the analytical calculation method for the calculation of inductance values will not work for a superconducting generator model.

Thus, using the parameters of the machine, many important values (e.g inductance) will be obtained using linear method and finite element analysis (FEM). Obtaining results for using FEM will be performed by using the software *COMSOL* along with *MATLAB*. This is done due to the non-linearity of the machine caused by the iron saturation.

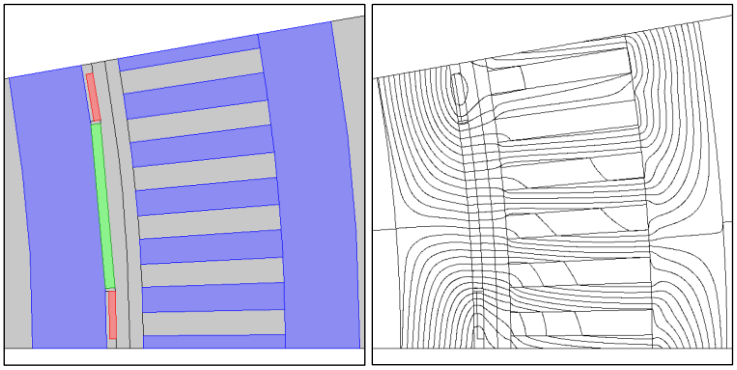

Figure 9: Generator Model in COMSOL

COMSOL is used for the numerical analysis of the SC machines to obtain all the inductance values for all the three generator topologies. There are three topologies that are compared and using the data for each of the individual topology, the COMSOL generator models are made. Figure 9 represents how a generator model is represented in the software.

For calculating the different inductance values, at first the armature and field area are calculated from the given dataset with their current densities are known. For calculating the field inductance (L_f) current is provided to the field winding while the rest of the currents are zero. The calculation of L_f requires the stator current (I_s) to be zero while only the field current (I_f) is injected into the field windings. Thus, only from the current I_f, there would be a flux linkage (λ_f) due to field current, from which it is possible to find the value of the inductance L_f.

$$L_f = \frac{\lambda_f}{I_f} \tag{3.21}$$

The shield inductances, L_{shd} and L_{shq}, are calculated analytically using Equation 2.22 [18]

$$\begin{aligned} L_{shd}, L_{shq} = & \frac{N_s^2 \cdot \mu_0 \cdot l \cdot \pi}{4 \cdot n \cdot p} \cdot \frac{1}{\left[1-(R_{s1}/R_{s2})^2\right]^2} \\ & \cdot \left[\frac{n \cdot p - 2 - (n \cdot p + 2) \cdot (R_{s1}/R_{s2})^4 + 4 \cdot (R_{s1}/R_{s2})^{n \cdot p + 2}}{(n \cdot p)^2 - 4} \right. \\ & \left. + 1 \cdot 2 \cdot \left(\frac{R_{s2}}{R_o}\right)^{2 \cdot n \cdot p} \cdot \left[\frac{1-(R_{s1}/R_{s2})^{n \cdot p + 2}}{(n \cdot p + 2)} \right]^2 \right], \end{aligned} \tag{3.22}$$

In equation 3.22,

- R_{s1} and R_{s2} represent the inner and outer radius of the shield respectively.

- R_o is the inside radius of the yoke.
- N_s represent the number of turns/ pole which is assumed to be 1.
- n represents the space harmonic order, which is considered to be the first space harmonic.
- I is either +1, -1 or 0 as the shield at radius R_o is ferrous, conductive or when no shield is present respectively. In this case, I is +1

For calculating L_d and Lq, at first the flux linkage (λ_{d_f}) is noted just due to the current provided by i_f into the field winding. After that, phase current a (i_{sa}) is provided to armature winding along with i_f at the field winding rated value. The new value of flux linkage (λ_{d_total}) is obtained. The total flux linkage (λ_{d_total}) is subtracted from the flux linkage due to the field current (λ_{d_f}) to obtain the flux linkage in the d-axis (λ_d). This is used to calculate the inductances L_d and L_q.

Steps:

1. Obtain λ_{d_f} only due to i_f.
2. Inject the current i_f and i_{sa} into the circuit to get λ_{d_total}.
3. Calculate L_d and L_q

$$L_d, L_q = \frac{\lambda_{d\_total} - \lambda_{d\_f}}{i_d} \tag{3.23}$$

Since the shield inductance values, $L_{shd,shq}$ are calculated using Equation 3.22, M_{a_f} is calculated by only providing the field current into the circuit as given in Equation 3.24.

$$M_{a\_f} = \frac{\lambda_d - i_d L_d}{I_f} \tag{3.24}$$

For calculating M_{f_shd} and M_{a_shd}, equation 3.6, 3.7 and 3.8 are used to solve as simultaneous equations for these values. In the generator model of *COMSOL*, only I_f is injected into the circuit *(i_d =0)* and the values of the flux linkage λ_d, λ_f and λ_{shd} are noted due to the field current only.

Using equation 3.6,

$$i_{shd} = \frac{\lambda_d - M_{a\_f} i_f}{M_{a\_shd}} \tag{3.25}$$

By putting value of i_{shd} in equation 3.26 and 3.27, the value of M_{a_shd} and M_{f_shd} can be calculated.

$$M_{a\_shd} = \frac{\lambda_{shd} - i_{shd} L_{shd}}{i_{shd}} \tag{3.26}$$

$$M_{f\_shd} = \frac{\lambda_{f} - i_{f} L_{f}}{i_{shd}} \tag{3.27}$$

Since the superconducting generator is a non-salient synchronous machine, all the inductance values in the d and q axis are equal.

The subtransient reactance X_d'' is calculated analytically using the equation 3.28 [24]

$$X_d'' = \frac{N_{ph}}{2} \cdot \left(\frac{X_d}{1.5} - \frac{w_e . L_{1d} . M_{a\_f}^2 - 2 . w_e . M_{af} . M_{a\_shd} . M_{f\_shd} + w_e . L_f . M_{a\_shd}^2}{L_{shd} . L_f - M_{f\_shd}^2} \right) \tag{3.28}$$

where N_{ph} represents the number of phases given as 3.

This calculation is made to check on the value of torque value after the short circuit. Since the value of the electromagnetic torque is inversely proportional to the value of the subtransient reactance, it can be checked whether the value of the short circuit torque is as expected or not.

Note that, distributed winding is used thus the value obtained from *COMSOL* for the flux density accounted for all the harmonic components as well. The assumptions for the model in this report only accounted for the values for sinusoidally distributed winding and thus the equations did not take into account all the harmonic components. A method is devised which allowed the user to obtain the fundamental component of the flux density to calculate the inductance.

3.4.2 A hybrid method (FEM for field computation, analytical for flux linkage)

The calculation using FEM provides us an accurate value as it takes into account all the harmonic components as well. As the entire generator model has been made on the basis sinusoidally distributed winding, it does not take into account the effects of the harmonic components. To overcome this, an idea is suggested which used a combination of both analytical and numerical methods for obtaining the inductances.

Figure 10 represents the magnetomotive force (mmf) distribution due to the distributed winding and has been compared to that of the fundamental sinusoidal winding.

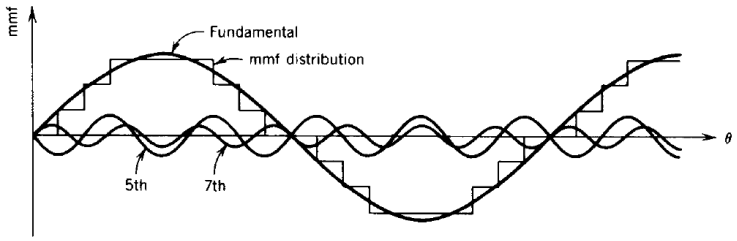

Figure 10: The mmf distribution due to distributed winding and ideal (Sinusoidal) distribution. [33]

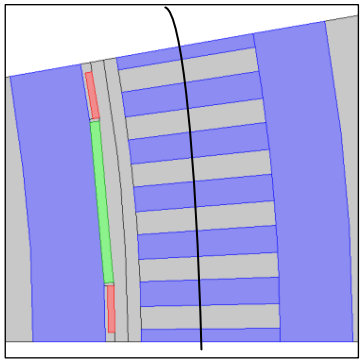

Figure 11: Flux Density waveform from the middle of the teeth for better averaging.

Figure 11 represents the location by using a black line from where the flux density waveform is obtained via COMSOL. It is only an approximation since the bottom of the teeth has the highest flux density and the upper part has the lowest thus the centre is chosen for a better averaging.

The steps that are followed to obtain the fundamental flux linkage value are given as follows:

1. Get flux density waveform data over one pole from COMSOL and then extend it to one pole pair.

2. Use FFT analysis in MATLAB to get the amplitude of the fundamental component of flux density obtained from 1.

3. Integrate the sinusoidal wave with the amplitude (obtained from 2) over one pole to get the flux linkage of one pole (be aware of the generator length and the number of turns). Then multiply this flux linkage per pole by the total number of poles.

4. Use this flux linkage to calculate the inductance.

This method allows us to use the assumptions that are made initially for the generator model to be sinusoidally distributed. This is a very important step towards the calculation of the parameters as they further accurately predicted the values to be more reliable considering the assumptions that are made in the beginning of the generator modelling. The next chapter shows all the values of inductance and resistances used for the three generator topologies.

3.5 Description of superconducting generators

There are three distinct topologies that are designed for the simulation. These three topologies are recommended and are modelled in COMSOL for FEM analysis. Figure 13 gives an idea about the construction of an SC generator and based on that the COMSOL model is made accordingly.

3.5.1 Why T1, T2 and T3?

The active material cost is taken into account for these three topologies and the value for their optimized variables as shown in **Table 5** is provided with the help of generic algorithm [31]. Figure 12 shows the cross section for a two pole SC synchronous generator.

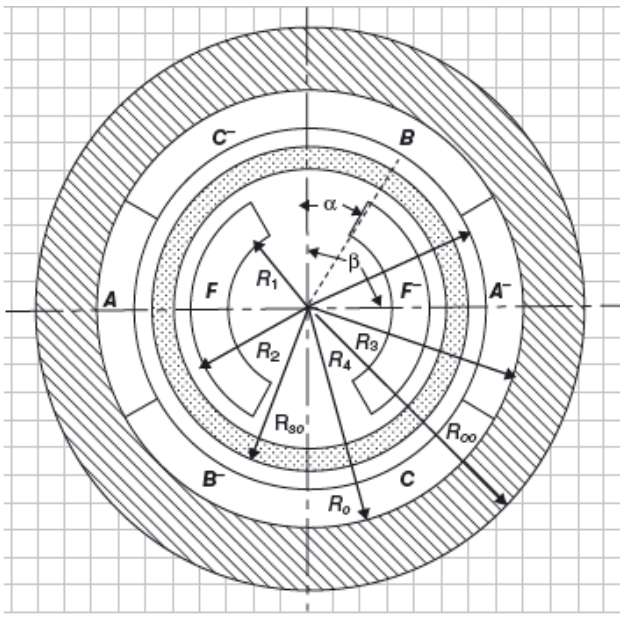

Figure 12: Two pole superconducting synchronous generator cross section.

- Where,

- F , F^+ represents field winding, positive and negative current regions
- A , A^- represents field phase A winding, positive and negative current regions
- B , B^- represents armature phase B winding, positive and negative current regions
- C , C^+ represents armature phase C winding, positive and negative current regions
- R_1 represents inside radius of field winding
- R_2 represents outside radius of field winding
- R_3 represents inside radius of armature winding
- R_4 represents outside radius of armature winding
- R_{so} represents outside radius of EM shield
- t_s represents radial thickness of EM shield
- R_o represents inside radius of yoke
- R_{oo} represents outside radius of yoke
- α represents the start angle of the field coil in degrees
- β represents the end angle of the field coil in degrees

Table 5 gives the variables which are given beforehand are also optimized for each of the three topologies. Figure 14 gives a comparison of the active material cost of the three topologies [33].

Table 5: Optimized variable values of each topology

Variables	T1	T2	T3
p	11	11	19
α [°]	38	50	62
β[°]	90	90	90
h_f[mm]	10	10	10
h_s [mm]	142	112	198
b_t/τ_s	0.2	0.2	0.52
h_{sy}[mm]	80	132	100
h_{ry} [mm]	80	162	100
l_s [m]	3.11	2.41	2.12

Where,

- p represents the number of pole pairs,
- α represents the start angle of the field coil in degrees
- β represents the end angle of the field coil in degrees
- h_f represents the field coil height in mm
- h_s represents the height of the armature slot mm
- b_t/τ_s represents the ratio of slot width/slot pitch
- h_{sy} represents the height of the armature yoke in mm
- h_{ry} represents the height of the field yoke in mm
- l_s represents the axial length of the generator in m.

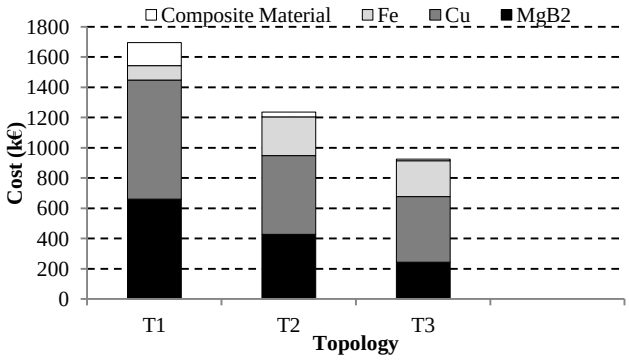

Figure 13: Active material cost comparison for T1, T2 and T3

As it can be seen from Figure 13 about how the cost is broken down for each of the topology. Details about the three generator topologies are discussed in the next section.

Note: It has to be remembered that although the generator characteristics from Table 4 are the same for all three topologies, the individual generator geometry differ in values as seen in Table 5.

3.5.2 Iron Armature Yoke (T1)

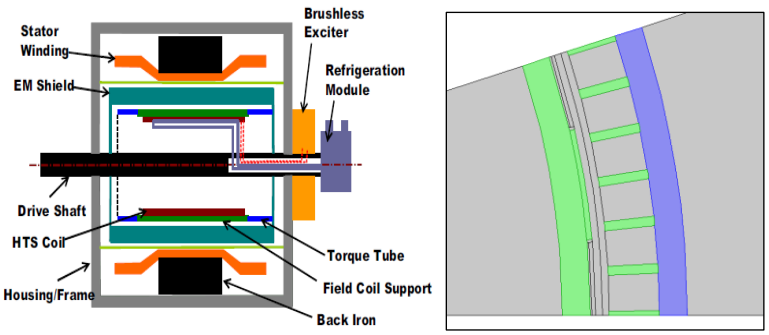

Figure 14: Iron armature yoke geometry and COMSOL model

The first topology that is modelled in COMSOL for obtaining the parameters is the Iron Armature Yoke topology. Figure 14 shows the configuration for T1. The field yoke, field pole core and the armature tooth are all made of non magnetic composite materials (NMC). The only part which consists of an iron part is the armature yoke on the outer radius of the stator. Figure 15 shows the generator model for this topology.

Advantage: The content of iron is the least in this topology and the mass of this generator topology will be the least as well compared to the rest.

Disadvantage: Usage of non-magnetic materials NMC will cost this generator topology the most out of all the three generator topology as seen from Figure 13.

3.5.3 Iron Yokes with Air Armature Teeth (T2)

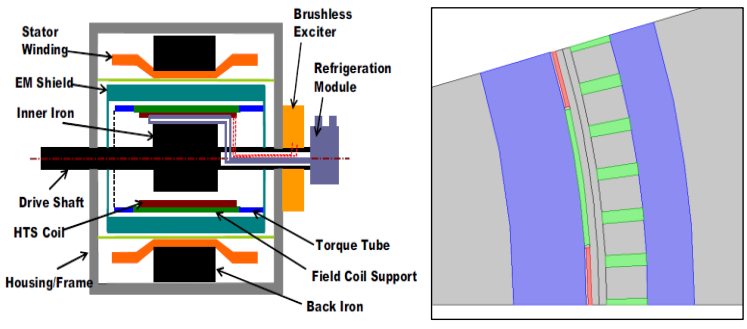

Figure 15: Iron yokes with air armature geometry and COMSOL model

The second topology that is modelled in COMSOL for obtaining the parameters is the Iron Yokes with Air Armature Teeth. The field pole core is non magnetic composite materials (NMC). The part which consists of the iron is the armature and the field yoke. Figure 15 shows the geometry and the COMSOL model for T2

Advantage: The content of iron is the available in the field yoke as well thus the mass of this generator topology will be higher compared to that of T1. The cost again will be lower than T1.

Disadvantage: Although there are less NMC materials in this topology due to increase in iron content, the generator will have more mass compared to T1.

3.5.4 Fully Iron Core (T3)

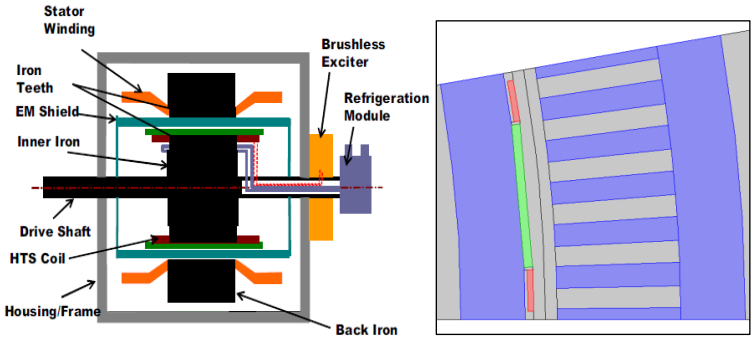

Figure 16: Fully iron core geometry and COMSOL model

The third and final topology that is modelled in COMSOL for obtaining the parameters is Fully Iron Core topology. The field pole core is made of non magnetic composite materials (NMC). The part which consists of an iron parts is the armature and the field yoke plus the armature teeth. Figure 17 shows the model that fulfils these parameters for the fully iron core.

Advantage: On a cost perspective, this topology has the least NMC materials thus will be the cheapest compared to the rest of the topologies.

Disadvantage: Due to the high content of iron the mass will be the highest for this machine. Also since there will be more copper content, the copper losses will be higher.

3.6 Parameter values

Table 6: Inductance Matrix T1

Iron Armature Yoke [T1] L- Matrix [H]				
0.0259	0	0.9216	$5.53x10^{-5}$	0
0	0.0259	0	0	$5.53x10^{-5}$
0.9216	0	93.14	$7.9x10^{-3}$	0
$5.53x10^{-5}$	0	$7.9x10^{-3}$	$8.29x10^{-5}$	0
0	$5.53x10^{-5}$	0	0	$8.29x10^{-5}$

Table 7 Inductance Matrix T2

Iron Yokes with air armature teeth [T2] L- Matrix [H]				
0.0167	0	1.21	$3.72x10^{-5}$	0
0	0.0167	0	0	$3.72x10^{-5}$
1.21	0	121.72	$13x10^{-3}$	0
$3.72x10^{-5}$	0	$13x10^{-3}$	$6.82x10^{-5}$	0
0	$3.72x10^{-5}$	0	0	$6.82x10^{-5}$

Table 8: Inductance Matrix T3

Fully Iron Core [T3] L- Matrix [H]				
0.0135	0	0.6324	$1.63x10^{-5}$	0
0	0.0135	0	0	$1.63x10^{-5}$
0.6324	0	42.58	$1.5x10^{-3}$	0
$1.63x10^{-5}$	0	$1.5x10^{-3}$	$9.07x10^{-5}$	0
0	$1.63x10^{-5}$	0	0	$9.07x10^{-5}$

The reason, as mentioned earlier, is due to the saturation effect provided by the iron in the machine which makes the inductance values non-linear. The FEM method allows for obtaining a more accurate value of inductance due to saturation and thus will give more accurate simulation of the transient performance. There are three models of different generator topologies that are modelled. Table 6, 7 and 8 show the inductance matrices for the three topologies [33]

Table 9: Resistance matrix for T1

Iron Armature Yoke [T1] R- Matrix [Ω]				
0.07	0	0	0	0
0	0.07	0	0	0
0	0	0.02	0	0
0	0	0	$2x10^{-3}$	0
0	0	0	0	$2x10^{-3}$

Table 10: Resistance Matrix for T2

Iron Yokes with air armature teeth[T2] R- Matrix [Ω]				
0.04	0	0	0	0
0	0.04	0	0	0
0	0	0.02	0	0
0	0	0	$2x10^{-3}$	0
0	0	0	0	$2x10^{-3}$

Table 11: Resistance Matrix for T3

Fully Iron Core [T3] R- Matrix [Ω]				
0.03	0	0	0	0
0	0.03	0	0	0
0	0	0.02	0	0
0	0	0	$2x10^{-3}$	0
0	0	0	0	$2x10^{-3}$

The resistance matrix represents all resistance values for d, q field and the shield. Table 9, 10 and 11 represents the resistance values calculated and obtained from all the three topologies.

It can be seen that R_f has always been considered to be 0.02Ω for all the three topologies [24]. Although the value can be much lower to almost zero for the field resistance, this value also includes the resistance in the current leads and the components of the exciter.

Chapter 4: Analysis of Transient Performance

4.1 Objectives and Assumptions

The objective of this chapter is to perform a transient and a load change analysis on the generator that has been modelled in Chapter 3.

There are two transient conditions that are simulated and analysed which are short circuit and load change characteristics. These two characteristics are implemented to study the transient performance of superconducting generators via comparing the short circuit torque to that of nominal torque for several topologies.

The three phase short circuit is simulated by making terminal voltage zero at a certain period of time. The load rejection is simulated by reducing the mechanical torque by 50% at a given point in time.

Before both the transient conditions, the generator is running at full load conditions.

4.2 Short Circuit Simulation (Full load condition)

A three phase terminal short circuit is considered to be one of the most serious faults that a generator can undergo. The simulations in this part of the chapter will give the results for four different conditions both before and after a three phase short circuit [34] [35].

4.2.1 Procedure & Assumptions

The short circuit is simulated by making the phase voltage zero, thus making U_d and U_q at a given point in time to create a three phase short circuit simulation. The short circuit is simulated at full load condition with the electromagnetic torque $[T_e]$ at $9.89\text{x}10^6$ N.m.

The effect is introduced at 2 s and four components of the model are compared.

- Torque

- Phase current
- Field current
- Speed

The condition for both before and after three phase short circuit will be shown in the results for the three generator topologies: T1, T2 and T3. The value of d-q currents are also compared to see their transient behaviour.

The three phase short circuit is applied to the generator when Us = 0 at 2 s. It is assumed that the generator is operating initially at rated load before the short circuit is applied. The value of the inertia is given as $6.01 \text{x} 10^7$ kg.m^2.

Another important issue which is not considered during the simulation is the value of the inductance remains constant throughout the whole procedure. In real life, this may change during transient conditions.

4.2.2 Results and discussions

The plots show the properties of field current, electromagnetic torque, phase current and the angular speed before and during a three phase short circuit. The results have been provided for T1, T2 and T3. Initially, the results will be shown for all three topologies. This will be followed by the reasoning behind the behaviour of the various components compared. The d-q currents will also be shown for seeing the behaviour of the circuit during this fault.

The three phase short circuit occurs at full load condition.

.

4.2.2.1 T1 Short Circuit simulation

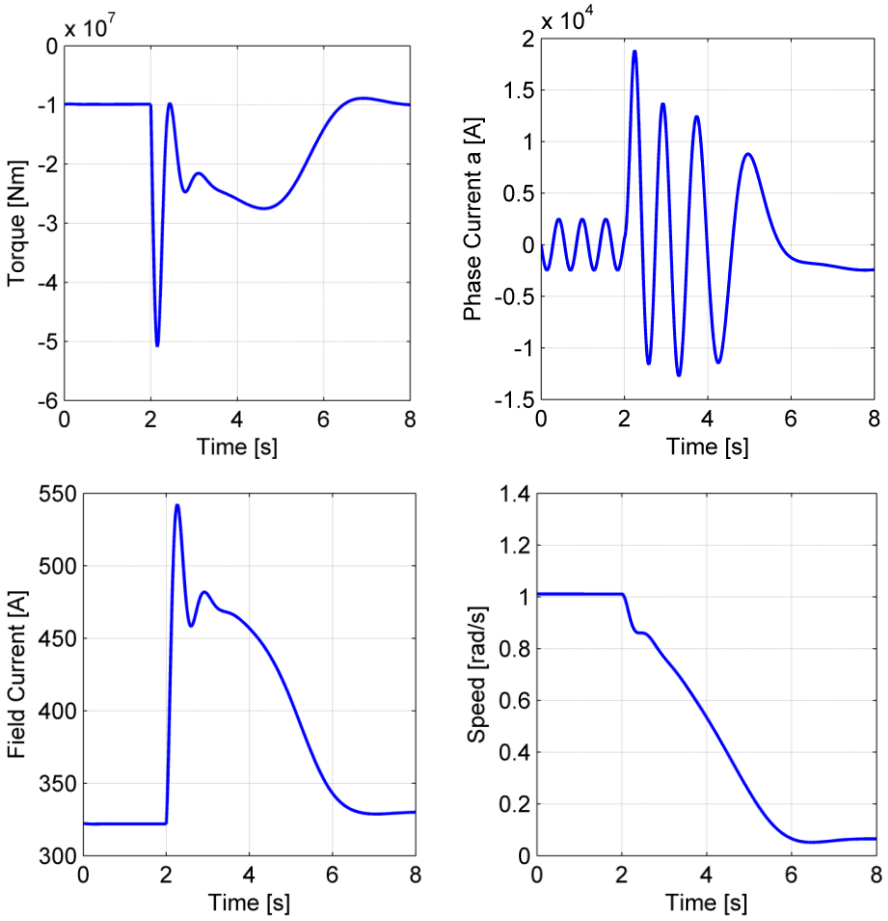

Figure 17: Short circuit characteristics for T1

Figure 17 represents the short circuit characteristics for the topology T1.

Torque: It is observed that the torque at 2 s goes to a peak value of around 5.0x10^7 N.m right after the short-circuit occurs and then oscillates back to its original position.

It is seen that the value of sub-transient reactance, X_d'' is calculated to be 0.2809 Ω from eq. 3.13 and since the magnitude of torque is inversely proportional to the value of X_d''. It can be seen that the torque during the short circuit is around 5 times the nominal torque, which satisfies the value of the inverse sub-transient reactance value.

Phase Current: Similar thing happens to the phase current as well. It can be seen that it reaches a peak of a little more than 18 kA. Due to the low sub-transient reactance of the generator, the phase current rises to a significant value of almost 8 times the rated current of the generator. It has to be noted that this is larger than the fault currents which occurs in a conventional machine.

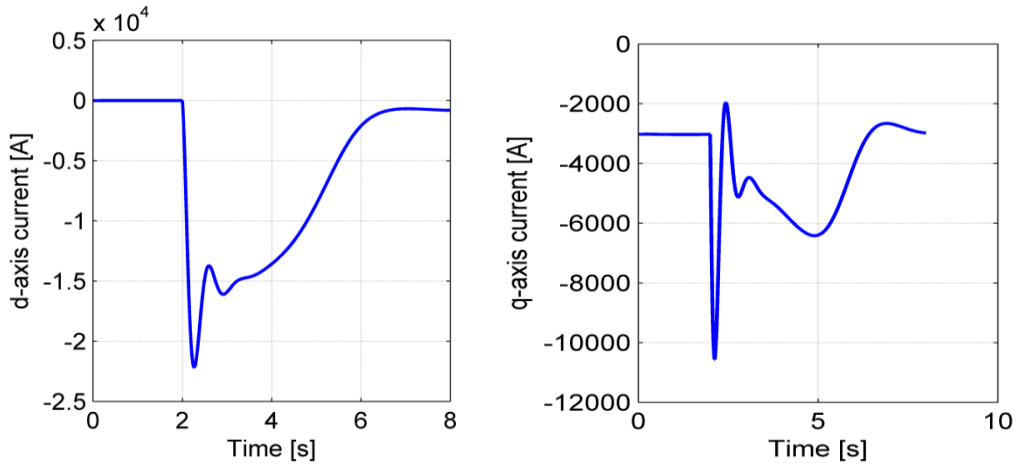

Figure 18: d-q current before and after short circuit

Field current: The short circuit is simulation shows the field current rises to 1.7 times the nominal value at 1s. It returns to the original position before the fault at 6 s.

Mechanical speed: The speed falls to minimum of 0.05 rad/s. Since the speed is reduced, the frequency of the machine will reduce as well. It can be seen from the graph of the phase current.

Discussion:

After the short circuit occurs, (u_d,u_q=0) the value of i_d and i_q will change as seen if Figure 18 . Since the value of i_d and i_q are 0 A and -3031 A respectively, their values will decrease and become further negative as the short circuit occurs. This matches with the requirements given in Equation 4.1 and 4.2 considering i_d and i_q are directly proportional.

$$u_d = R_s i_d - pw_m \lambda_q \tag{4.1}$$

$$u_q = R_s + pw_m \lambda_d \tag{4.2}$$

Before the short circuit, the flux linkages of the field winding and shield [λ_f, $\lambda_{shd,q}$] are constant. No current is present in the shield winding because it rotates as the same speed as the synchronous speed [31] [32].When the short circuit occurs, armature current flows whose magnetomotive force (mmf) directly oppose the mmf of the field winding. The flux linkages of both field winding and shield winding are affected. To maintain field and shield fluxes at their initial values (Lenz's Law), induced components of currents will flow in both field winding and shield winding. This can be seen from equation 4.3 and 4.4

$$\lambda_f = L_f i_f + M_{a\_f} i_d + M_{f\_\mathrm{shd}} i_{\mathrm{shd}} \tag{4.3}$$

$$\lambda_{\mathrm{shd}} = L_{\mathrm{shd}} i_{\mathrm{shd}} + M_{f\_\mathrm{shd}} i_f + M_{a\_shd} i_{\mathrm{shd}} \tag{4.4}$$

As the value of i_d becomes negative, the value of i_f must rise at that instant to keep the fluxes at their initial values. Thus i_f rises as seen from the results in Figure 17.

This induced current in the field and shield winding causes a rise in current amplitude when the fault occurs. The current in these windings decay because of the resistances R_f, R_{shd} and R_{shq} in these circuits. These induced currents are equivalent to an increase of the field excitation, and therefore a large current will flow in the stator circuit immediately after the short circuit.

Due to the high value of current, a large torque is also produced of around 5 times the nominal value. Since the value if T_m is constant and value of T_{em} rises to a high value, the speed of the machine will reduce to almost zero. Thus, the frequency of the machine will reduce as well.

4.2.2.2 T2 Short Circuit simulation

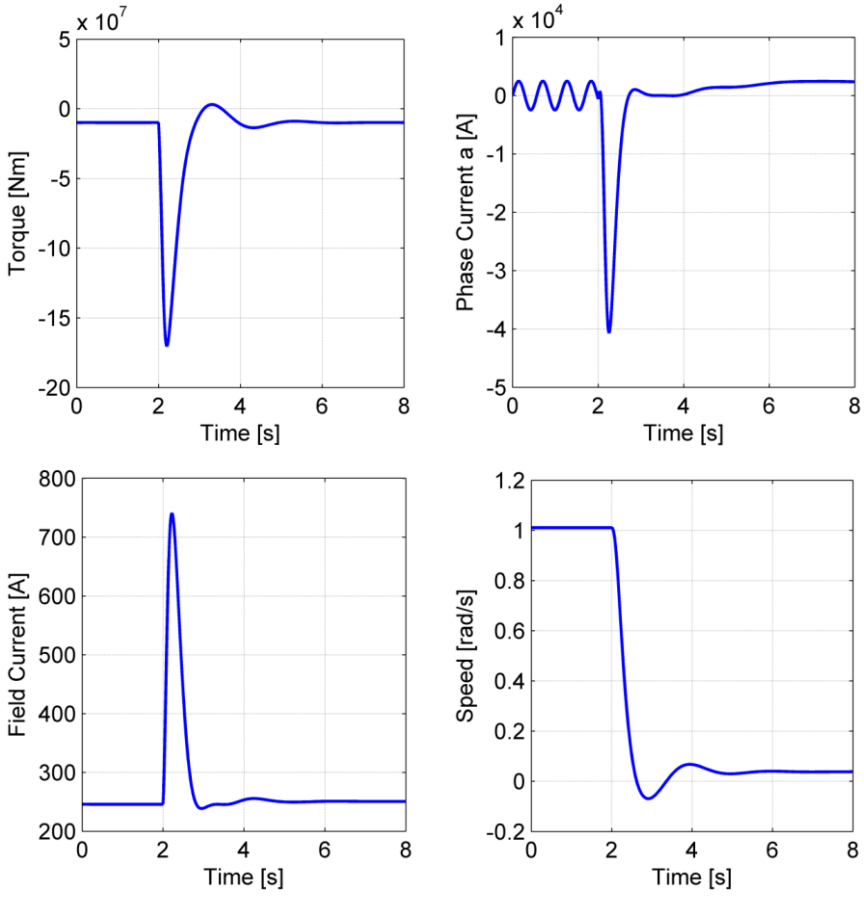

Figure 19: Short circuit characteristics for T2

The topology T2 has more content of iron than T1 and it can be seen that this topology in general has a lower synchronous reactance than T1 as seen in Table 6 and 7. Figure 19 represents the short circuit characteristics for the generator topology T2.

Torque: The torque goes to a negative peak value of around 17x10^7 N.m and then oscillates back to a value higher than that of the original position. Before returning to the original position at 3 s, T_{em} becomes positive thus going into motor operation for around 0.5 s as seen in Figure 20. The peak amplitude has a higher magnitude than T1. It is seen that the value of sub-transient reactance, X_d'' is calculated to be 0.077 Ω and since the magnitude of torque is inversely proportional to the value of X_d''. (Note: This is a simple check and is not completely accurate as the value of X_d'' is calculated analytically thus saturation is not taken into account) It can be seen that the torque during the short circuit is around 16 times the nominal torque, which satisfies the value of the inverse sub-transient reactance value.

Phase current: The phase current goes up to 40 kA which is almost 16 times the nominal value. Due to an even lower value the low sub-transient reactance of the generator, the phase current rises to a significant value of around 16 times the rated current of the generator. The magnitude is higher mainly due to the fact that the sub-transient reactance is even lower than T1. The frequency for this topology changes the most.

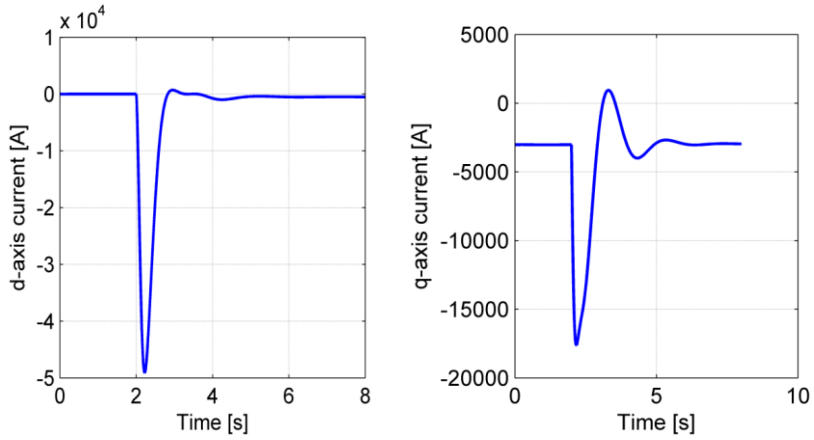

Figure 20: T2 d-q current after short circuit

Field current: The short circuit is simulation for T2 shows the field current rises to 12 times the nominal value at 2 s It returns to the original position before the fault at 3 s.

Mechanical speed: Since the torque rises to a high value of 16 times the nominal value, the machine goes below zero for a while at 3 s and returns to a positive value at 5 s with a speed around *0.02 rad/s.*

Discussion: The discussion for this topology is similar to that of the topology of T1. The only difference is that the short circuit torque is much higher during the fault and the machine goes into motor operation for around *0.5 s.*

4.2.2.3 T3 Short Circuit simulation

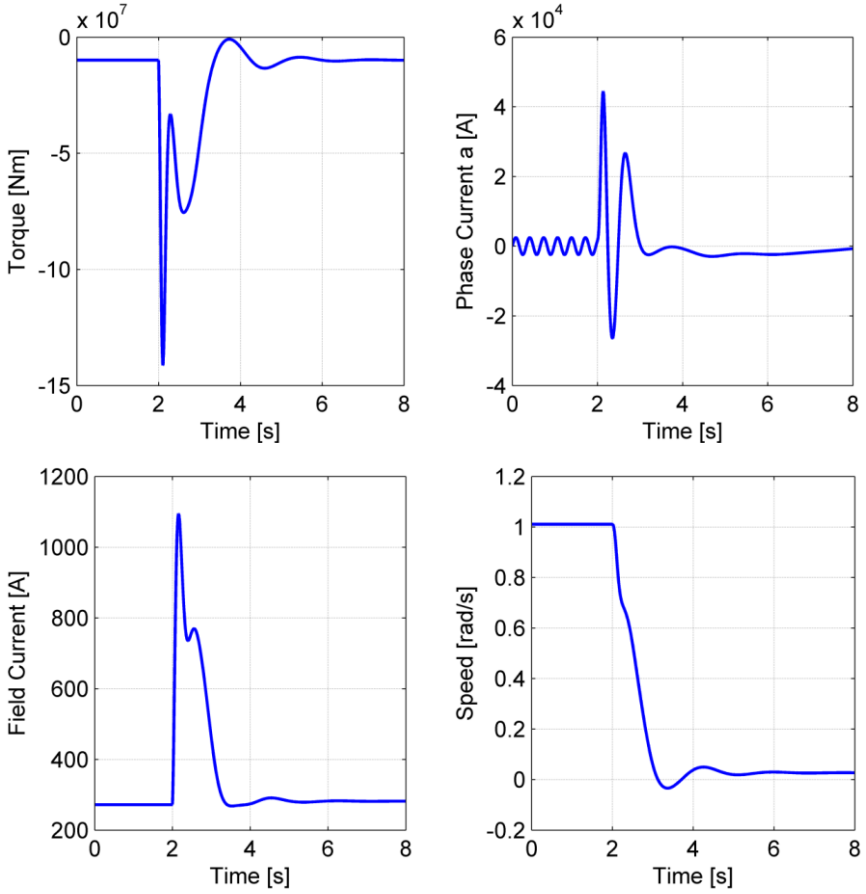

Figure 21: Short circuit characteristics for T3

The Fully Iron Core topology T3 has the most content of iron compared to both T1 and T2. It can be seen that T3 has the lowest synchronous reactance compared to the rest of the topologies as seen in Table 6, 7 and 8. Figure 21 represents the short circuit characteristics for the generator topology T2.

Torque: The torque goes to a negative peak value of around 14.4×10^7 N.m and then oscillates back to a value higher than that of the original position. This peak amplitude is has a higher magnitude than T1 but lower than that of T2. It is seen that the value of sub-transient reactance, X_d'' is calculated to be 0.118 Ω and since the magnitude of

torque is inversely proportional to the value of X_d''. It can be seen that the torque during the short circuit is around 14 times the nominal torque, which satisfies the value of the inverse sub-transient reactance value.

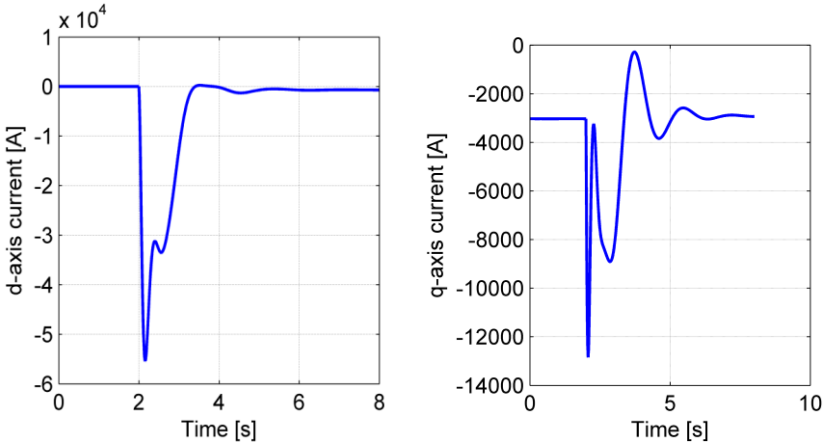

Figure 22: T3 d-q current after short circuit

Phase current: The phase current goes up to 45 kA and keeps oscillating at that position. Again, due to the low sub-transient reactance of the generator, the phase current rises to a significant value of around 18 times the rated current of the generator. This magnitude is the highest compared to T1 and T2.

Field current: The short circuit is simulation for T2 shows the field current rises to 4.7 times the nominal value at 1s. It reaches a steady state value of around 1100 A after 1.5 s after the three phase short circuit is provided to the circuit. This value is higher than both T1 and T2.

Mechanical speed: Similarly as T2, since the torque rises to a high value of 14.4 times the nominal value, the machine goes below zero for a while at 3 s and returns to a positive value at 5 s with a speed around *0.01 rad/s*

Discussion: The discussion for this topology is similar to that of the topology of T1 and T2. The only difference is that the short circuit torque is much higher during the fault and the machine goes into motor operation for around *0.5 s.*

4.2.3 Data Comparison

Table 12: Torque comparison T1, T2 and T3

Short Circuit	T1	T2	T3
Nominal Torque [N.m]	$9.9x10^6$	$9.9x10^6$	$9.9x10^6$
Peak Torque	$50\ x10^6$	$160\ x10^6$	$144\ x10^6$
Peak/ Nominal	5.05	16.17	14.55

It can be seen that T2 has the highest rate of increase in torque during short circuit of more than 16 times. It can also be seen from the change of the frequency and speed drop during the transient period. The sub-transient reactance also has the lowest value for T2 thus indicating higher value of short circuit current. The electromagnetic torque rises very quickly to a high value thus creating reduction in speed. Both T2 and T3 go to motor operation for a while when the value of T_{em} goes above zero.

In all of the cases above, it is seen that the speed has reduced indicating that the electromagnetic torque is higher than the mechanical torque during the three phase short circuit. Thus the speed continues to decrease before the torque reaches a steady state value. Usually, in a conventional machine, the speed almost remains constant as the average torque over the transient period is almost similar to that of steady state. Also in a conventional generator, the electrical time constant of the machine is much smaller than the mechanical time constant thus the speed almost remains constant. But for the DDSCG in this report, the electrical time constant of the machine is not significantly smaller than the mechanical time constant of the machine. This maybe one of the reasons for which the speed reduces significantly during a fault as the T_e increases.

T3 has the highest increase in field current value. Although the critical current density is not known in this case, this high current might cause damage or may even take away the superconducting property of the field windings.

T1 is the least affected out of all the topologies with a higher value of sub-transient reactance with the peak torque only reaching 5 times compared to that of 16 and 14.5 for T2 and T3 respectively

In this scenario, T1 would be a safer option to implement as a generator topology due to its better performance during a three phase short circuit. It has the least increase in peak torque during the three phase short circuit.

4.3 Load rejection simulation

This generator may experience a sudden load change due to the drop in the electromagnetic torque, T_e. When the load reduces, the pitch of the blade in the wind turbine also changes accordingly to reduce the mechanical torque, T_m to that value. In this simulation, a 50% load rejection is simulated during a full load condition and the effects on the three generator topologies are seen.

A sudden load change in the operating condition of for a synchronous generator connected to a power system may result in loss of synchronism. It is important to predict the ability of a synchronous machine to remain in synchronism after a disturbance occurs. The load rejection simulation conducted in this section is a disturbance that is not as severe as a three phase short circuit. It will be seen how the superconducting generator model will perform during this disturbance

4.3.1 Procedure & Assumptions

For load rejection is simulated by reducing the T_m by 50% at 2 s. Therefore, the T_e also changes and the magnitude reduced by 50% by changing the pitch of the blade.

Since an actual pitch controller and a wind turbine model are not used for simulating the change in the mechanical load, T_m, this is replaced by using a ramp with a saturation block. The ramp had the initial output with the nominal torque, T_{nom} thus running at full load. For reducing T_m by half, the ramp uses a negative slope to make sure that the torque reduces linearly to half the value of T_{nom}. The saturation block made sure that the torque did not reduce further than the value that of $T_{nom}/2$. Figure 23 shows the characteristics of the mechanical torque during steady state full load condition and after the load rejection at 2 s.

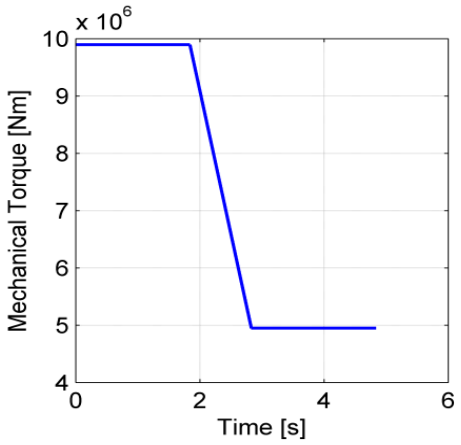

Figure 23: For simulating load torque

The following criteria will be observed for the load rejection simulation.

- Torque
- Phase current
- Field current
- Speed

The condition for both before and after the load change will be shown in the results for comparing their transient performance. This is done for all the three generator topologies. It is assumed that the generator is directly connected to the grid via the converters. For a load rejection, the time period for the transient is much slower than that of a three phase short circuit.

- Generator side converter: d-q voltage controller on the generator side for terminal voltage. This makes sure that the maximum power is obtained from the generator via controlling the voltage.
- Grid side converter: This controls the reactive power and the active power is controlled via the pitch controller as mentioned above.

The following statements are taken into consideration.

- The terminal voltage, V_t, is assumed to be of constant since the generator is connected to the grid.
- The field voltage, u_f, is also constant

- The electrical frequency, w_e, is constant throughout since the machine is connected to the grid.
- Current is leading the voltage according to the graph of the phase a current and voltage.
- Emf is constant due to constant speed and field current.
- Since the generator is paralleled to the grid the values such as frequency and phase of the voltage do not change.
- The angle between the emf and the terminal voltage (δ) will change accordingly when there is a load change.

4.3.1.1 Generator side controller

The controller as shown in Figure 24 makes sure that the maximum power available from the DDSSG is obtained at all times. This is done by using the measured d-q currents and measured speed as input, and the d-q voltage as output.

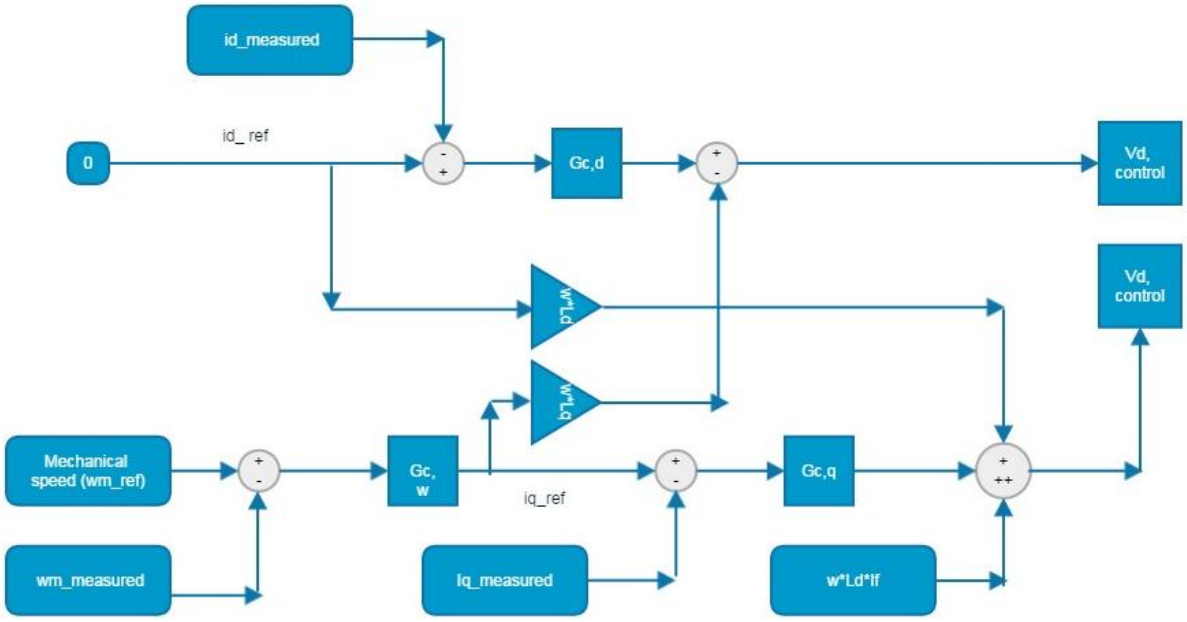

Figure 24: D-q voltage controller diagram

The controller uses three inputs which are

- d-axis current measured (i_d)
- q-axis current measured (i_q)
- Mechanical speed measured (w_m)

Appendix B shows a more detailed figure of the block and its components.

These inputs uses the PI controller $G_{c,d}$, $G_{c,q}$ and $G_{c,w}$ for obtaining the controlled d and q axis voltage, V_d and V_q. They are also mentioned and described in Appendix B [9].

4.3.2 Results and discussions

Load rejection is simulated at 2 s after the electromagnetic torque is reduced by 50%. Eq. 4.5 represents value of the emf.

$$\mathrm{E}=\frac{\mathrm{w}_e \mathrm{M}_{af} \mathrm{I}_f}{\sqrt{2}} \tag{4.5}$$

Where

- w_e represents the electrical frequency
- M_{af} represents the mutual inductance between the armature and field windings.
- I_f represents the field current.

M_{af} is constant throughout the situations. Since the speed is not constant, and field current changes as well, the e.m.f value will change after the load rejection.

The load rejection will be later explained by using a phasor diagram. It is expected that all the three topologies will behave similarly during a 50% load rejection.

Since the current is leading the voltage for all the three topologies before the load rejection occurs. This means that the reactive power is being supplied to the generator.

4.3.2.1 T1 50% Load rejection

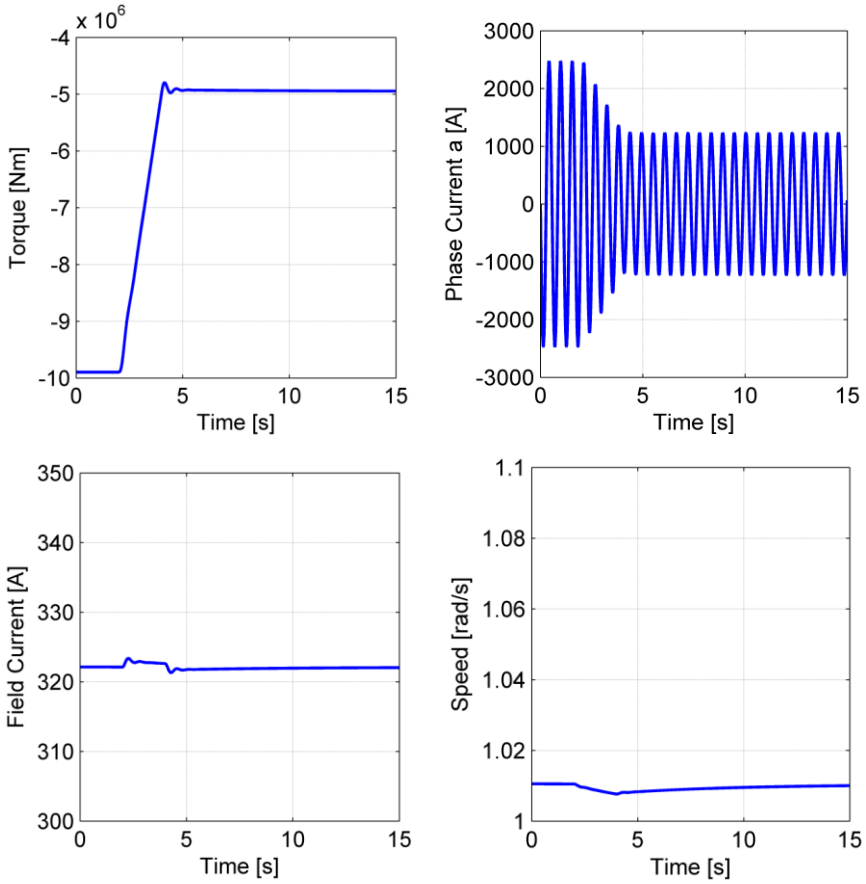

Figure 25: T1 Load rejection characteristics

It can be seen that the 50% load rejection causes a drop in phase current A, i_a, to reduce by half from 2500 A to 1250 A. From Figure 25, it can be seen that both the field current, i_f, and the mechanical speed, w_m, are almost constant both during the entire period. This means that the emf is also constant during this mode of operation.

The electromagnetic torque, T_e, reduces by half. Since the output power will reduce by 50% as well and w_m is a constant speed before and after the transient period, thus the torque reduces exactly by half as well. Figure 27 shows how the reactive power changes after the load reduction. The reactive power is controlled by the grid side converter.

$$\mathrm{Q} = u_{\mathrm{q}} i_{\mathrm{d}} - u_d i_q \tag{4.6}$$

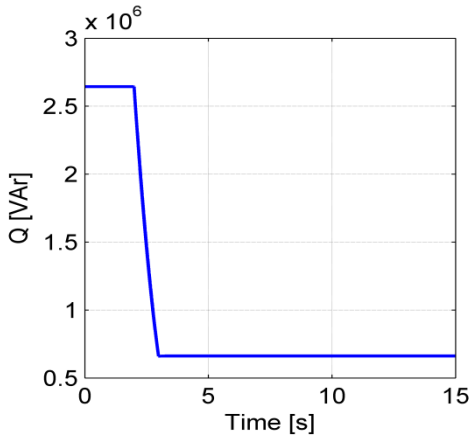

Figure 26: Reactive power for T1 before and after load rejection

Equation 4.6 shows the relationship of the reactive power with the d-q voltage and currents. This shows that both the active and the reactive power are controlled.

4.3.2.2 T2 50% Load rejection

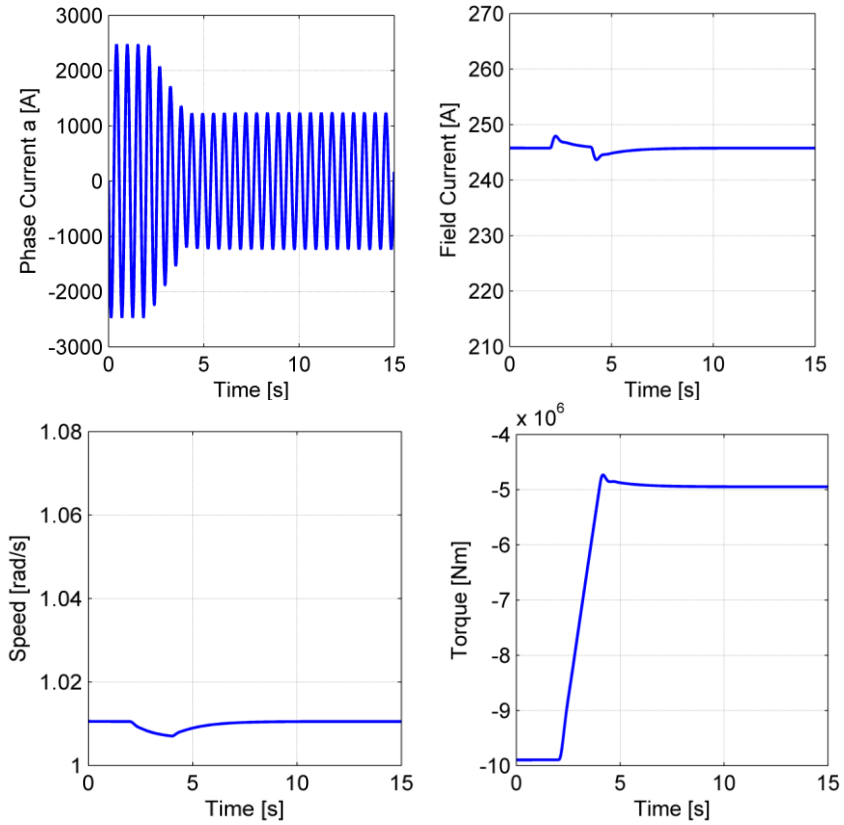

Figure 27: T2 Load rejection characteristics

The generator topology T2 also faces similar consequences as both i_a, T_e and the output power, $P_{m,}$ is halved as seen from Figure 27. The field current is still constant during the entire period. As mentioned earlier, w_m remains constant during before and after

the load rejection. Also the field current, i_f, is also constant. It only changes slightly while the load torque is reducing to half the value.

This causes a similar result for T2 as it is for T1 where the current reduces to 1250 A.

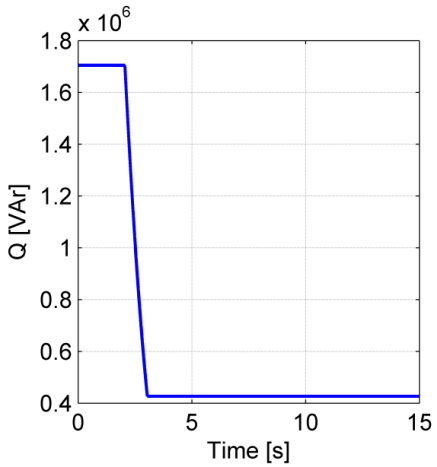

Figure 28: Reactive power for T2 before and after load rejection

Similarly as T1, the reactive power is controlled along with the active power after the load rejection as shown in Figure 28.

4.4.2.3 T3 50% Load rejection

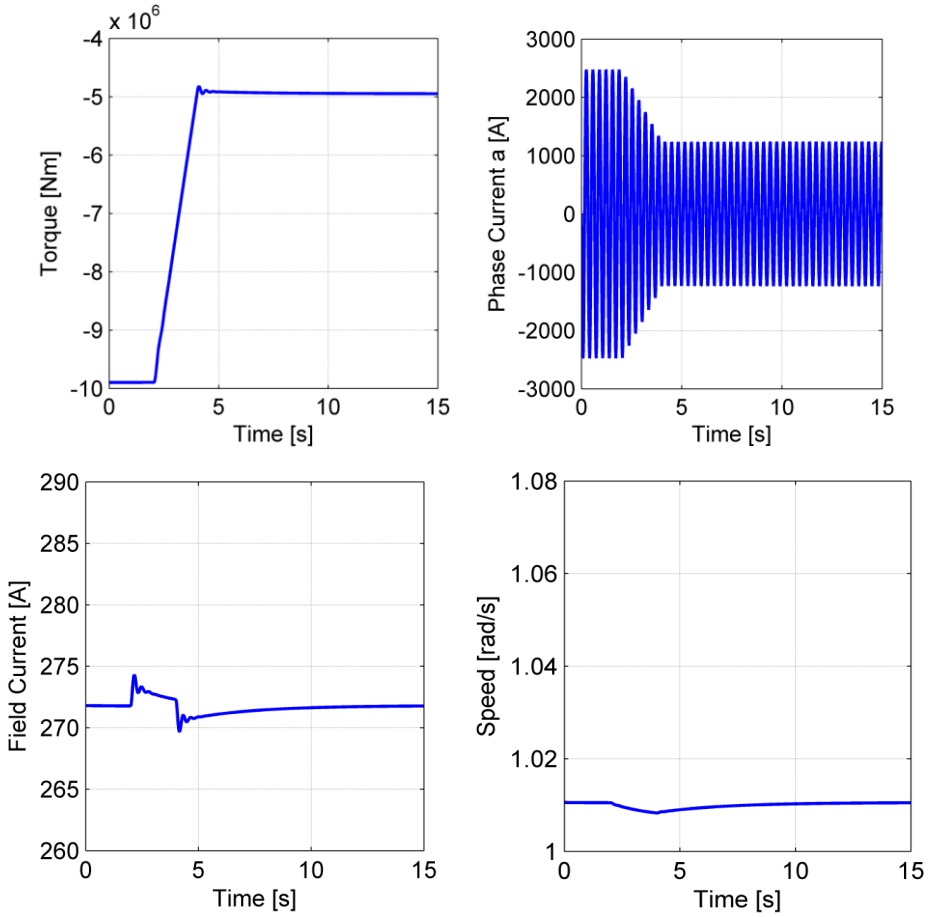

Figure 29: T3 load rejection characteristics

T3 also shows the same results as T1 and T2 where both i_a, T_e and the output power, $P_{m,}$ is halved as seen from Figure 29. By observing the value of the speed and the field current, it can be said that the e.m.f is constant in this case as well. T3 the current is leading the voltage by 12.5°.

The current is leading in this case as well and it can be seen that the current reduces after the load rejection.

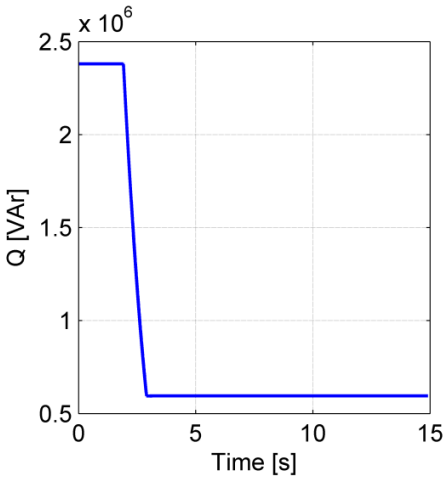

Figure 30: Reactive power for T3 before and after load rejection

T3 shows the same characteristics as T1 and T2 as the reactive power is controlled along with the active power after the load rejection as shown in Figure 30.

Discussions:

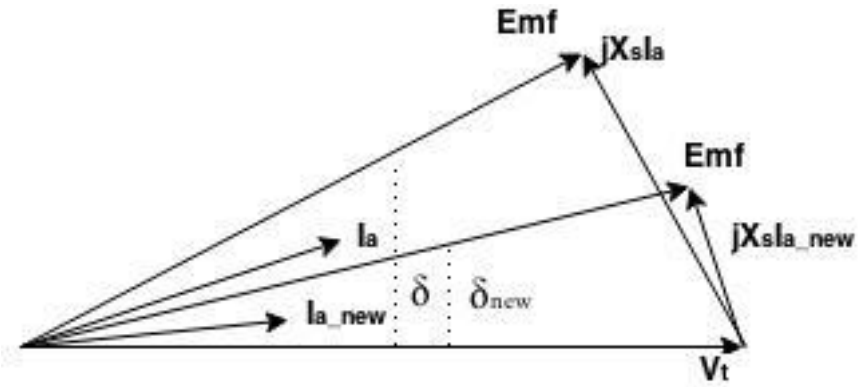

Figure 31: Phasor diagram for SC generator (Generator connected to the grid)

It can be seen that all the topologies have performed similarly during a 50% load. Since the generator is connected to the grid, the value of phase voltage and frequency are unchanged due to the grid.

From the phasor diagram in Figure 31, I_{new} represent the new current value after the load rejection.. Angle, δ, between e.m.f (E) and terminal voltage V_t reduces after the load rejection to a smaller value δ_{new}. Thus the value of $Esin\,\delta$ will reduce overall.

Since both the field current, I_f and the speed of the generator, w_e, is constant, the e.m.f will be constant as well. Now since the current is already leading the voltage by 15.7°, 10° and 12.5° for T1, T2 and T3 respectively, a decrease in δ will actually cause the

current to decrease in magnitude. Thus the stator current has to increase in magnitude as seen from the phasor diagram.

In short, for T1, T2 and T3 the phase current decreases in all three cases. Since the current is leading for all the three generator topologies, according to the phasor diagram, a load rejection will cause a decrease in current since the terminal voltage and emf are constant.

The active and the reactive power are controlled accordingly. The generator is connected to the grid with all the requirements fulfilled.

For all three topologies, the current is still leading the voltage but the angle θ_{new} the load rejection is smaller than θ after the load rejection. Therefore the current becomes less leading after a 50% load rejection for all the three topologies. This can be seen as after the load rejection, the amount of reactive power injected into the generator reduces since the current becomes less leading. This occurs for all the topologies.

It can be seen that all the topologies have performed similarly during a 50% load rejection with d-q voltage controller. The mechanical speed, field current and e.m.f is made to be constant due to the controller.

Chapter 5: Conclusion and Recommendation

5.1 Comments on models and superconducting machines

After modelling the generator for T1, T2 and T3 a three phase short circuit and load change simulation is performed on the models.

Short circuit in generator terminal causes problems as they can produce excess current in the field winding and damage the rotor SC field. This fault is considered to be amongst the most severe faults the generator operates through. It can be seen that the initial peak value of the torque for all the three generator models are quite high compared to that of a conventional machine and might cause problems in the machine dynamics. Generator topology T2 showed the highest peak torque during the short circuit going up to more than 16 times the nominal torque. This might be dangerous for the generator as it might destroy the mechanical parts of the turbine. Also the high value of current in the stator may cause excessive heat and may damage the thermal insulation.

T3 shows the highest increase in field current during the three phase short-circuit by increasing up to 5 times the rated value. This might damage the MgB_2 windings and may cause it to lose its superconductivity. As the critical current density is not calculated, it is not exactly known how it might damage the windings.

On the basis of the generator topology, T1 gets affected the least during three phase short circuit. It can be said that it is a better option in terms of torque and field current characteristics compared to T2 and T3.

But then again, even though the content of iron in T1 is low, the higher content of NMC causes T1 to be more expensive than both T2 and T3.

T2 and T3 on the other hand are more cost efficient but as mentioned before, their ability to actually perform during a transient performance has a higher risk compared to that of T1.

During the 50% load rejection simulation on the generator models. The constant I_f and w_m causes the emf to be constant. As the current is leading before the load rejection, the slight drop in the terminal voltage in T1, T2 and T3 causes the current to increase

in magnitude as shown in Figure 32 phasor diagram. The amount of reactive power injected into the generator reduced in all the three cases as the current became less leading with the voltage.

Although the current carrying ability for superconducting machines is quite amazing, it has to be understood that such machines under transient behaviour will show a large amount of current which may even destroy the wind turbine materials due to excess torque. The three topologies that are tested are just a proposed idea to see the behaviour in a closer manner.

The flowchart in **Figure 32** gives the reader an idea on the steps followed to obtain the results.

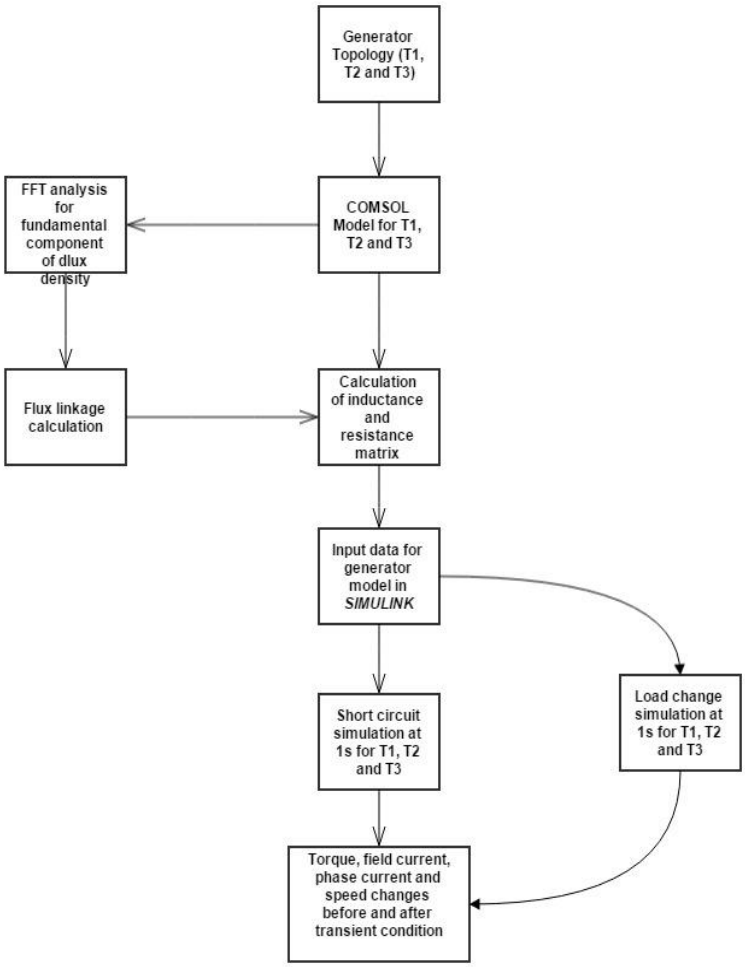

Figure 32: Flowchart of parameter calculations and simulations

5.3 Recommendations

There are several recommendations and issues to be brought forward for future work. This report did not take several issues into account and recommends more study on them:

- The inductance is assumed to be constant both before and during the three phase short circuit. This might not be true as the value might change during the fault. Further research should be made into this by making inductance variable during transients.
- Due to lack of controllers, the mechanical speed and the field current is assumed to be constant during the load rejection. Although a terminal voltage controller is used, due to constant mechanical speed, both the torque and power are halved. For future work, more controllers should be taken into account for better approximation and accurate results.
- There are two generator models made for testing the transient and load change characteristics. One model for simulating three phase short circuit. The other one for simulating 50% load rejection. The functioning of these models could be verified further by using the energy conservation method to check if the model makes sense. If the energy is not conserved then it means that the model is incorrect.
- Another issue which is not investigated in this report is to compare the fault current for the field winding with the critical current. This can be done by comparing the critical current value before and after the fault with that of the field current for the same condition. This will allow the user to check if the material crosses its critical limit which might cause it to lose its superconductivity.

These are some issues which are not taken into consideration in this report and might be used for future work.

The technology of superconducting machines is advancing every year and the effort to implement it into wind turbines is already being made by companies such as AMSC. This report tries to give the reader an idea about how an SC wind turbine generator would perform during faults and load changes.

Generator topologies such as T1 will give further hope to the research field for further implementing the idea of having a 10MW or larger SC wind turbine in the near future.

Bibliography

[1] Council, G. W. E. (2014). Annual installed global capacity 1996-2013. Retrieved 07/2014, 2014, from http://www.gwec.net/global-figures/graphs/

[2] Corbetta, G. (2014). The European offshore wind industry- key trends and statistics 2013 (pp. 22): European Wind Energy Association.

[3] Edenhofer, O., Pichs-Madruga, R., Sokona, Y., Seyboth, K., Matschoss, P., & Kadner, S. (2011). Special Report on Renewable Energy Sources and Climate Change Mitigation (pp. 1075). United Kingdom and New York, NY, USA: IPCC.

[4] Gamble, B., Snitchler, G., & Kalsi, S. S. (2006). HTS Generator Topologies. *American Superconductor Corporation*, 1-5.

[5] Jensen, B. B., Mijatovic, N., & Abrahamsen, A. B. (2012). Development of Superconducting Wind Turbine Generators. *Invited Paper*.

[6] Umans, S. D. (2009). Transient performance of a High-Temperature-Superconducting generator. *IEEE*, 451-457.

[7] Chun, Y. D., Lee, H. W., Lee, J., Kwon, Y. K., Ryu, K. S., & HonG, J. P. (1999). Transient Analysis of a Superconducting AC Generator using the compensated 2-D Model. *IEEE TrANSACTIONS ON MAGNETICS, 35*(5), 4085-4087.

[8] E, A. M., Alolah, A., & M., H. (2013). Maximum Power Extraction from Utility-Interfaced Wind Turbines *INTECH* (pp. 160-192).

[9] L, Q. (2012). *Modelling and Simulation of Grid-connected Superconducting Wind Turbine Generators.* (Doctor of Science), Tokyo University, Tokyo, Japan.

[10] Slootweg, J. G. (2003). Wind Power Modelling and Impact on Power System

Dynamics. (Doctorate Doctoral Thesis), TU Delft, Delft, Netherlands.

[11] Fu, X., Chen, Z., & Zhang, J. (2008). Pitch Angle Control for Variable Speed Wind Turbines. *DRPT, 6*(9), 6.

[12] Al-Hawa, C. (2006). Methods For Determination Of The Excitaion Current In Synchronous Generators (E. Design, Trans.) (Vol. X-ETS/EEK-0309). Stockholm, Sweden: KTH.

[13] Dr, W. (2013). Superconductors - An Introduction. Retrieved from Azom website: http://www.azom.com/article.aspx?ArticleID=941

[14] Terao, Y., Sekino, M., & Ohsaki, H. (2013). Comparison of Conventional and Superconducting Generator Concepts for OffshoreWind Turbines. *IEEE TRANSACTIONS ON APPLIED SUPERCONDUCTIVITY, 23*(3), 1-4.

[15] Sharma, D. (2009). *Investigation on transient performance of Superconducting generator with governor control* (Master of Engineering), THAPAR UNIVERSITY, Patiala, Indida. (147004)

[16] Abrahamsen, A. B., & Jensen, B. B. (2012). Superconducting Direct Drive Wind Turbine Generators: Advantages and Challenges. In S. M. Muyeen (Ed.), *Wind Energy Conversion Systems. Technology and trends.* (pp. 53-80). Springer Publishing Company. (Green Energy and Technology).

[17] Liu, Y., Qu, R., Zhe, Z., Wang, J., & Fang, H. (2014). Analysis on the Performanace of a Rotor Screen for a 12 MW Superconducting Direct-drive Wind Generator. *IEEE TRANSACTIONS ON APPLIED SUPERCONDUCTIVITY, 24*(5), 5.

[18] Kalsi, S. S. (2014). Superconducting Wind Turbine Generator Employing MgB_2 Windings Both on Rotor and Stator. *IEEE TRANSACTIONS ON APPLIED SUPERCONDUCTIVITY, 24*(1).

[19] Polinder, H., Genani, G., Liu, D., & Kostopoulos, D. (2014). Feasibility Study of a 10 MW MgB_2 Fully Superconducting Generator for Offshore Wind Turbines

(pp. 11). Mekelweg 4, 2628CD Delft, Netherlands: Delft University of Technology.

[20] Kalsi, S. S., Weeber, K., Takesue, H., Lewis, C., Neumueller, H.-W., & Blaugher, R. D. (2004). Development status of rotating machines employing superconducting field windings. *Inviter Paper, IEEE, 92*(10), 1688-1704.

[21] K. Vinod, Neson. V, & Syamaprasad, U. *Development of MgB2 Superconductors with Improved Superconducting Properties* (Vol. 3): Materials and Minerals Division, National Institute for Interdisciplinary Science and Technology.

[22] Vinod, K., & Syamaprasad, U. (2006). Prospects for MgB2 superconductors for magnet application. *IOP Publishing Ltd, 20*(1). doi: 10.1088/0953-2048/20/1/R01

[23] Kalsi, S. S. (2013). Rotating AC Machines *Applications of High Temperature Superconductors to Electric Power Equipment* (pp. 93-94): Wiley.

[24] Kalsi, S. S. (2013). Rotating AC Machines *Applications of High Temperature Superconductors to Electric Power Equipment* (pp. 95-97): Wiley.

[25] Keysan, O. (2013). *Electrical drives for direct drive renewable energy systems.*

[26] Qu, R., Liu, Y., & Wang, J. (2013). Review of Superconducting Generator Topologies for Direct-DriveWind Turbines. *IEEE TRANSACTIONS ON APPLIED SUPERCONDUCTIVITY, 23*(3), 5201108

[27] Polinder, H., Ferreira, J. A., Jensen, B. B., Abrahamsen, A. B., Atallah, K., & McMahon, R. A. (2013). Trends in wind turbine generator systems. *IEEE JOURNAL OF EMERGING AND SELECTED TOPICS IN POWER ELECTRONICS, 1*(3), 174-185.

[28] Awad, M. L. (1999). *Modeling of Synchronous Machines for System Studies.* (PhD), University of Toronto, Toronto, Canada. (0-612-41092-7)

[29] Spoljaric, Z., Miklosevic, K., & Jerkovic, V. Synchronous generator modeling

using Matlab. *Faculty of Electrical Engineering, University of Osijek, Croatia.*

[30] Hoeijmakers, M. J. (2004). *Modelling of AC machines* H. Paling (Ed.) (pp. 101).

[31] Chapman.S. (2012). Electric Machinery Fundamentals: BAE Systems. Australia.

[32] Sen, P. C. (1997). *Principles of electric machines and power electronics*. New York: Wiley.

[33] Liu, D., & Polinder, H. (2014). Comparison of 10 MW Superconducting Generator Topologies for Wind Turbines. TU Delft

[34] Chun, Y. D., Kim, Y. H., Kim, S., & Lee, J. (2002). Transient analysis of superconducting generator under the three phases of sudden grounding fault condition. *Department of Electrical Engineering, Hanyang University.*

[35] Oyetola, J. B. (2012). Analysis Of Symmetrical Short-Circuit Current And Performance Of Synchronous Generators. *IJERT, 1*(9), 10.

[36] Kim, G. H., Kim, N., Kim, K. M., Park, M., Yu, I. K., Lee, S., & Park, T. J. (2012). EMTDC Based Simulation of 10 MW Class Grid-Connected Superconducting Wind Turbine Generator. *IEEE TRANSACTIONS ON APPLIED SUPERCONDUCTIVITY, 22*(3), 5.

Appendix A-Generator Model

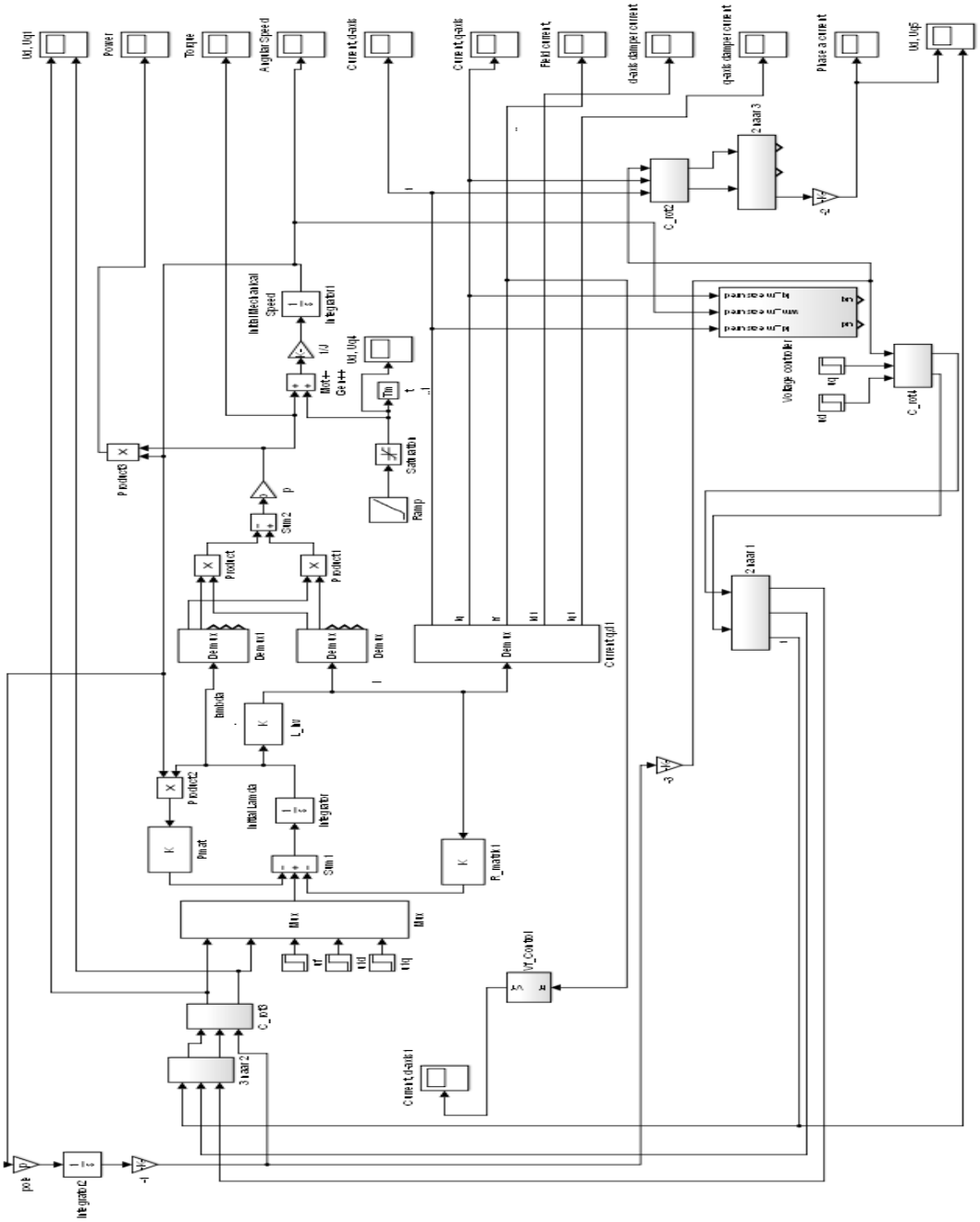

Figure 33: Superconducting synchronous generator model

Figure 33 represents the SC synchronous generator model. The controller is not attached but is shown in the model.

Appendix B- Controller model for d-q voltage

Figure 34 represents the overview and the *MATLAB/ SIMULINK* model of the d-q voltage controller. (Loic Queval Thesis)

A decoupled control is defined by defining the feedback loops and controllers $G_{c,d(s)}$, $G_{c,q(s)}$ and $G_{c,w(s)}$.

$$v_{stq,ctrl} = G_{c,q}(s)(i^*_{stq} - i_{stq,meas}) + \omega_e L_d i^*_{std} + \omega_e L_{md} i'^*_f$$

$$v_{std,ctrl} = G_{c,d}(s)(i^*_{std} - i_{std,meas}) - \omega_e L_q i^*_{stq}$$

The parameters of the PI controller is

$$G_c(s) = K_p \frac{1 + T_i s}{T_i s}$$

The controller is tuned as shown in Table 13

Table 13: Controller tuning for d-q voltage

	w_c [rad/s]	a	K_p [si]	T_i [s]
$G_{c,d(s)}$	$2\pi * f_{PWM}/20$	$1/(w_c * T_a)$	$(T_d * R_s)/(a * T_a)$	$a^2 * T_a$
$G_{c,q(s)}$	-	4	$(T_d * R_s)/(a T_a)$	$a^2 * T_a$
$G_{c,w(s)}$	-	4	$2*J/(3*p*L_d*i_f*a_w*T_{eq})$	$a^2 * T_{eq,q}$

In Table 13, f_{PWM} is given as 1000 Hz.

T_a is given is $1/f_{PWM}$

Table 14, 15 and 16 gives the controller parameters for the three generator topologies: T1, T2 and T3.

Using the values of the controller, the d-q voltages are tuned for controlling the terminal voltage while keeping the speed and the field current constant. This also keeps the emf at a constant value.

Table 14: Controller values for T1

	w_c [rad/s]	a	K_p [si]	T_i [s]
$G_{c,d(s)}$	314.15	3.18	8.14	0.01
$G_{c,q(s)}$	-	4	6.47	0.016
$G_{c,w(s)}$	-	4	$1.1x10^{7}$	0.15

Table 15: Controller values for T2

	w_c [rad/s]	a	K_p [si]	T_i [s]
$G_{c,d(s)}$	339.29	3.18	5.67	$9x10^{-3}$
$G_{c,q(s)}$	-	4	4.50	0.015
$G_{c,w(s)}$	-	4	$2.36x10^{7}$	0.15

Table 16: Controller values for T3

	w_c [rad/s]	a	K_p [si]	T_i [s]
$G_{c,d(s)}$	339.29	3.18	4.58	$9x10^{-3}$
$G_{c,q(s)}$	-	4	3.64	0.015
$G_{c,w(s)}$	-	4	$1.53x10^{7}$	0.15

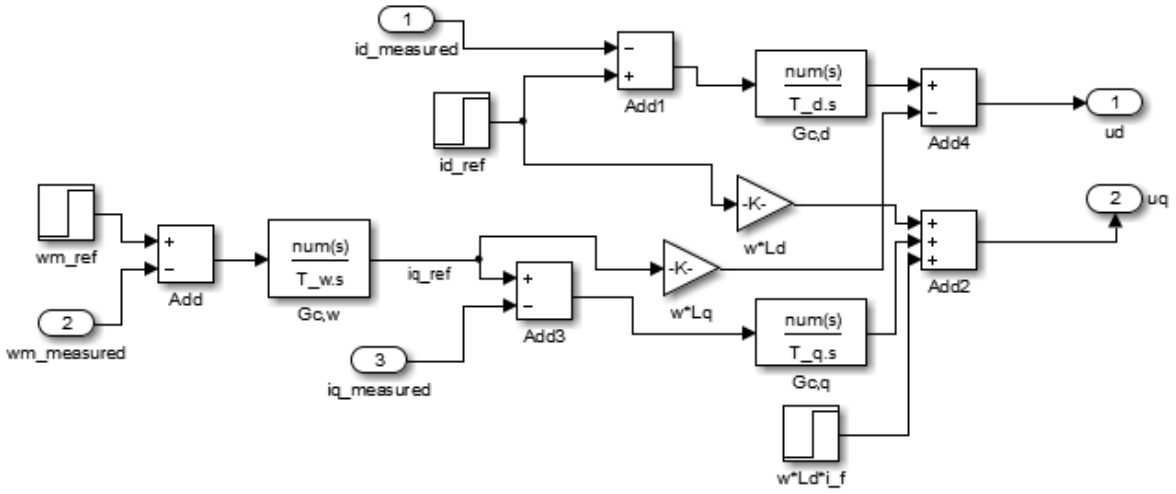

Figure 34: Simulink model of the voltage controller

Appendix C- MATLAB

```
clear all
clc

%Superconducting generator

Us=3300/sqrt(3)/1.00;     %Phase Voltage
U1=2628.7/sqrt(2);

p=11;                     %Number of pole pairs
f_m=9.65/60;              %Mechanical Frequency
f=f_m*p;                  %Electrical Frequency
Pm=10e6;                  %Given Mechanical Power
t=40;                     %Time taken to reach nominal speed


fi0=pi/2-0.274;           %Phase of voltage u_a at t=0
w_m=2*pi*f/p;             %Mechanical speed (rad/s)
w=2*pi*f;                 %Electrical Speed (rad/s)

T=Pm/w_m;                 %Nominal torque calculated from power
J=5.0083e7*1.2;           %Calculating inertia from calculated torque and
time taken to reach nominal speed

sl=(T/2-T)/2;             %Slope for the reduction of mechanical torque

om0=w_m;                  %Mechanical Speed at t=0
oms=om0*p;                %Stator frequency at t=0


pmat_new=  [0 -p 0 0 0;
            p 0 0 0 0;
            0 0 0 0 0;
            0 0 0 0 0;
            0 0 0 0 0]

Rs=0.061*1.089;
Rf=0.02;                     %From Kalsi

R_1d=3.04709e-6;             %Test d-axis damper winding resistance
R_1q=3.04709e-6;             %Test q-axis damper winding resistance

T_mech=3*3031^2*Rs/w_m;
```

```
Rmat=[Rs 0 0 0 0;
     0 Rs 0 0 0 ;
     0 0 Rf 0 0;
     0 0 0 R_1d 0;
     0 0 0 0 R_1q];        %The resistance matrix for simulink

Ld=0.0259;
Lq=0.0259;%0.24*1.089/w;
L_1d=1.7145e-7*(2*p)^2;%(3.39463e-5+2.67902e-5)/2;%2.58623e-5  Distributed
anc concentrated winding average inductance
L_1q=1.7145e-7*(2*p)^2;%(3.39463e-5+2.67902e-5)/2;

Lf=93.138; %103.63; %54.8806; %121.57; %Field Inductance
Msf=0.9581*pi/4*sqrt(3/2);%*1.5*pi/4;%1.15;%0.63714/1.067*1.2; %Mutual
inductance calculated from via COMSOL


Mf_1d=1.6404e-5*2*p*2*p;%(0.03394+0.01056)/2; %Damper winding same number
of turns as stator
Mf_1q=1.6404e-5*2*p*2*p;%(0.03394+0.01056)/2;

Ms_1d=2.0553e-6*2*p*sqrt(3/2);%(5.63101e-4+1.874e-4)/2; %Damper winding
same number of turns as stator
Ms_1q=2.0553e-6*2*p*sqrt(3/2);%(5.63101e-4+1.874e-4)/2;

L_new=[Ld 0 Msf Ms_1d 0; %The inductance matrix for simulink
       0 Lq 0 0 Ms_1q;
       Msf 0 Lf Mf_1d 0;
       Ms_1d 0 Mf_1d L_1d 0;
       0 Ms_1q 0 0 L_1q];

pi_new=pi;
i_f=Us*sqrt(3)/(pi_new*2*f*Msf); %Calculated initial
                                  %excitation Field current from AC
                                  %machines


uf=i_f*Rf;       %Calculated excitation voltage

%When machine is connected to the inifinite bus,
%E=U=400
E=3300/sqrt(3);
Xd=(w)*Ld;

emf=w_m*Msf*i_f/sqrt(2);

T_po=(3*Us*E)/(w_m*Xd); %Pull out torque for the overall synchronous
machine

P_nom=w_m*T_po %Nominal power of the manchine- Can be reached if excitation
voltage is increased
```

```
id=0;
iq=-3031;


%Imat=[0 3031 i_f 0 0]'; %Current matrix for initial loaded condition

Imat=[id iq i_f 0 0]'; %Current matrix for initial condition
psi0_new=L_new*Imat; %For generating initial conditions for the Synchronous
generator

ud=Rs*id-p*w_m*Ld*iq;
uq=Rs*iq+(Msf*i_f+Ld*id)*p*w_m;


iq_sc=(-Msf*i_f*p*w_m)/(Rs+Ld*p^2*w_m^2*Ld/Rs);
id_sc=p*w_m*Ld*iq_sc/Rs;



Q=-ud*iq;

xd_tr=1.5*(w*Ld-((Msf^2)*(w)/Lf));
xd_sub=(3/2)*((w*Ld)-((L_1d*Msf^2-2*Msf*Ms_1d*Mf_1d-Lf*Ms_1d^2)*(w)/...
(L_1d*Lf-Mf_1d^2)));

%CONTROLLER

f_pwm=1000; % Given value
Ta=1/f_pwm;
Teq=0.15/16;   %Assumed from page 86
w_c=2*pi*f_pwm/20;

tau_d=Ld/Rs;
tau_q=Lq/Rs;
tau_f=Lf/Rf;

a_d=1/(w_c*Ta);
a_q=4;
a_w=4;
a_f=a_d;

Kp_d=tau_d*Rs/(a_d*Ta);
Kp_q=tau_q*Rs/(a_q*Ta);
Kp_w=2*J/(3*p*Ld*i_f*a_w*Teq);
Kp_f=tau_f*Rf/(a_f*Ta);

T_d=a_d^2*Ta;
T_q=a_q^2*Ta;
T_w=a_w^2*Teq;
```

```
T_f=a_f^2*Ta;


sim('Finalmodel')
%time = Torque.Time(2238:end)- Torque.Time(2238);
figure(1)
width = 3;     % Width in inches
height = 3;    % Height in inches
alw = 0.75;    % AxesLineWidth
fsz = 11;      % Fontsize
lw = 1.5;      % LineWidth
msz = 8;       % MarkerSize
pos = get(gcf, 'Position');
set(gcf, 'Position', [pos(1) pos(2) width*100, height*100]); %<- Set size
set(gca, 'FontSize', fsz, 'LineWidth', alw); %<- Set properties
set(gcf,'InvertHardcopy','on');
set(gcf,'PaperUnits', 'inches');
papersize = get(gcf, 'PaperSize');
left = (papersize(1)- width)/2;
bottom = (papersize(2)- height)/2;
myfiguresize = [left, bottom, width, height];
set(gcf,'PaperPosition', myfiguresize);
plot(Torque1(:,1),Torque1(:,2),'LineWidth',lw);grid on;%title('Torque after
a load change of 50% at 1s');
xlabel('Time [s]'); ylabel('Torque [Nm]')
print('T4_SC_torque','-dpng','-r800');

figure(2)
width = 3;     % Width in inches
height = 3;    % Height in inches
alw = 0.75;    % AxesLineWidth
fsz = 11;      % Fontsize
lw = 1.5;      % LineWidth
msz = 8;       % MarkerSize
pos = get(gcf, 'Position');
set(gcf, 'Position', [pos(1) pos(2) width*100, height*100]); %<- Set size
set(gca, 'FontSize', fsz, 'LineWidth', alw); %<- Set properties
set(gcf,'InvertHardcopy','on');
set(gcf,'PaperUnits', 'inches');
papersize = get(gcf, 'PaperSize');
left = (papersize(1)- width)/2;
bottom = (papersize(2)- height)/2;
myfiguresize = [left, bottom, width, height];
set(gcf,'PaperPosition', myfiguresize);
plot(Fieldcurrent1(:,1),Fieldcurrent1(:,2),'LineWidth',1.5);grid
on;%title('Field Current after a load change of 50% at 1s');
ylim([300 350])
xlabel('Time [s]'); ylabel('Field Current [A]')
print('T4_SC_fieldcurrent','-dpng','-r800');

figure(3)
width = 3;     % Width in inches
height = 3;    % Height in inches
```

```
alw = 0.75;     % AxesLineWidth
fsz = 11;       % Fontsize
lw = 1.5;       % LineWidth
msz = 8;        % MarkerSize
pos = get(gcf, 'Position');
set(gcf, 'Position', [pos(1) pos(2) width*100, height*100]); %<- Set size
set(gca, 'FontSize', fsz, 'LineWidth', alw); %<- Set properties
set(gcf,'InvertHardcopy','on');
set(gcf,'PaperUnits', 'inches');
papersize = get(gcf, 'PaperSize');
left = (papersize(1)- width)/2;
bottom = (papersize(2)- height)/2;
myfiguresize = [left, bottom, width, height];
set(gcf,'PaperPosition', myfiguresize);
plot(Phasecurrent1(:,1),Phasecurrent1(:,2),'LineWidth',1.5);grid
on;%title('Phase Current after a load change of 50% at 1s');
%axis([0 5])
xlabel('Time [s]'); ylabel('Phase Current a [A]')
print('T4_SC_phasea','-dpng','-r800');

figure(4)
width = 3;      % Width in inches
height = 3;     % Height in inches
alw = 0.75;     % AxesLineWidth
fsz = 11;       % Fontsize
lw = 1.5;       % LineWidth
msz = 8;        % MarkerSize
pos = get(gcf, 'Position');
set(gcf, 'Position', [pos(1) pos(2) width*100, height*100]); %<- Set size
set(gca, 'FontSize', fsz, 'LineWidth', alw); %<- Set properties
set(gcf,'InvertHardcopy','on');
set(gcf,'PaperUnits', 'inches');
papersize = get(gcf, 'PaperSize');
left = (papersize(1)- width)/2;
bottom = (papersize(2)- height)/2;
myfiguresize = [left, bottom, width, height];
set(gcf,'PaperPosition', myfiguresize);
plot(Angularspeed1(:,1),Angularspeed1(:,2),'LineWidth',1.5);grid
on;%title('Phase Current after a load change of 50% at 1s');
ylim([1 1.1])
xlabel('Time [s]'); ylabel('Speed [rad/s]')
print('T4_SC_angspeed','-dpng','-r800');

figure(5)
width = 3;      % Width in inches
height = 3;     % Height in inches
alw = 0.75;     % AxesLineWidth
fsz = 11;       % Fontsize
lw = 1.5;       % LineWidth
msz = 8;        % MarkerSize
pos = get(gcf, 'Position');
set(gcf, 'Position', [pos(1) pos(2) width*100, height*100]); %<- Set size
set(gca, 'FontSize', fsz, 'LineWidth', alw); %<- Set properties
```

```
set(gcf,'InvertHardcopy','on');
set(gcf,'PaperUnits', 'inches');
papersize = get(gcf, 'PaperSize');
left = (papersize(1)- width)/2;
bottom = (papersize(2)- height)/2;
myfiguresize = [left, bottom, width, height];
set(gcf,'PaperPosition', myfiguresize);
plot(Tm1(:,1),Tm1(:,2),'LineWidth',1.5);grid on;%title('Phase Current after
a load change of 50% at 1s');
%axis([0 5])
xlabel('Time [s]'); ylabel('Mechanical Torque [Nm]')
print('T4_SC_Tm','-dpng','-r800');

figure(6)
width = 3;     % Width in inches
height = 3;    % Height in inches
alw = 0.75;    % AxesLineWidth
fsz = 11;      % Fontsize
lw = 1.5;      % LineWidth
msz = 8;       % MarkerSize
pos = get(gcf, 'Position');
set(gcf, 'Position', [pos(1) pos(2) width*100, height*100]); %<- Set size
set(gca, 'FontSize', fsz, 'LineWidth', alw); %<- Set properties
set(gcf,'InvertHardcopy','on');
set(gcf,'PaperUnits', 'inches');
papersize = get(gcf, 'PaperSize');
left = (papersize(1)- width)/2;
bottom = (papersize(2)- height)/2;
myfiguresize = [left, bottom, width, height];
set(gcf,'PaperPosition', myfiguresize);
plot(Currentd(:,1),Currentd(:,2),'LineWidth',1.5);grid on;%title('Phase
Current after a load change of 50% at 1s');
xlabel('Time [s]'); ylabel('d-axis current [A]')
print('T4_SC_d','-dpng','-r800');

figure(7)
width = 3;     % Width in inches
height = 3;    % Height in inches
alw = 0.75;    % AxesLineWidth
fsz = 11;      % Fontsize
lw = 1.5;      % LineWidth
msz = 8;       % MarkerSize
pos = get(gcf, 'Position');
set(gcf, 'Position', [pos(1) pos(2) width*100, height*100]); %<- Set size
set(gca, 'FontSize', fsz, 'LineWidth', alw); %<- Set properties
set(gcf,'InvertHardcopy','on');
set(gcf,'PaperUnits', 'inches');
papersize = get(gcf, 'PaperSize');
left = (papersize(1)- width)/2;
bottom = (papersize(2)- height)/2;
myfiguresize = [left, bottom, width, height];
set(gcf,'PaperPosition', myfiguresize);
```

```
plot(Currentq(:,1),Currentq(:,2),'LineWidth',1.5);grid on;%title('Phase
Current after a load change of 50% at 1s');
xlabel('Time [s]'); ylabel('q-axis current [A]')
print('T4_SC_q','-dpng','-r800');


figure(4)
width = 3;     % Width in inches
height = 3;    % Height in inches
alw = 0.75;    % AxesLineWidth
fsz = 11;      % Fontsize
lw = 1.5;      % LineWidth
msz = 8;       % MarkerSize
pos = get(gcf, 'Position');
set(gcf, 'Position', [pos(1) pos(2) width*100, height*100]); %<- Set size
set(gca, 'FontSize', fsz, 'LineWidth', alw); %<- Set properties
set(gcf,'InvertHardcopy','on');
set(gcf,'PaperUnits', 'inches');
papersize = get(gcf, 'PaperSize');
left = (papersize(1)- width)/2;
bottom = (papersize(2)- height)/2;
myfiguresize = [left, bottom, width, height];
set(gcf,'PaperPosition', myfiguresize);
plot(Angularspeed1(:,1),Angularspeed1(:,2),'LineWidth',1.5);grid
on;%title('Phase Current after a load change of 50% at 1s');
%axis([0 5 1 1.1])
xlabel('Time [s]'); ylabel('Speed [rad/s]')
print('T4_50_angspeed_no_controller','-dpng','-r800');

figure(5)
width = 3;     % Width in inches
height = 3;    % Height in inches
alw = 0.75;    % AxesLineWidth
fsz = 11;      % Fontsize
lw = 1.5;      % LineWidth
msz = 8;       % MarkerSize
pos = get(gcf, 'Position');
set(gcf, 'Position', [pos(1) pos(2) width*100, height*100]); %<- Set size
set(gca, 'FontSize', fsz, 'LineWidth', alw); %<- Set properties
set(gcf,'InvertHardcopy','on');
set(gcf,'PaperUnits', 'inches');
papersize = get(gcf, 'PaperSize');
left = (papersize(1)- width)/2;
bottom = (papersize(2)- height)/2;
myfiguresize = [left, bottom, width, height];
set(gcf,'PaperPosition', myfiguresize);
plot(Tm1(:,1),Tm1(:,2),'LineWidth',1.5);grid on;%title('Phase Current after
a load change of 50% at 1s');
%axis([0 5])
xlabel('Time [s]'); ylabel('Mechanical Torque [Nm]')
print('T4_50_Tm_no_controller','-dpng','-r800');

figure(6)
```

```
width = 3;      % Width in inches
height = 3;     % Height in inches
alw = 0.75;     % AxesLineWidth
fsz = 11;       % Fontsize
lw = 1.5;       % LineWidth
msz = 8;        % MarkerSize
pos = get(gcf, 'Position');
set(gcf, 'Position', [pos(1) pos(2) width*100, height*100]); %<- Set size
set(gca, 'FontSize', fsz, 'LineWidth', alw); %<- Set properties
set(gcf,'InvertHardcopy','on');
set(gcf,'PaperUnits', 'inches');
papersize = get(gcf, 'PaperSize');
left = (papersize(1)- width)/2;
bottom = (papersize(2)- height)/2;
myfiguresize = [left, bottom, width, height];
set(gcf,'PaperPosition', myfiguresize);
plot(time,Q.Data(2223:end),'LineWidth',1.5);grid on
xlabel('Time [s]'); ylabel('Q [VAr]')
print('T4_50_q','-dpng','-r800');
```